SEISMIC DATA PROCESSING REPORT

Geological Survey of Western Australia South-West 1 Deep Crustal 2D

23GSWA-SW1

REV, DATE	REV1, 8 MAY 2024
PREPARED BY	REECE CUNNOLD
REVIEWED BY	JAI KINKELA

EXECUTIVE SUMMARY

HiSeis conducted the acquisition and processing of deep crustal, 2D seismic reflection data for the Geological Survey of Western Australia (GSWA). The project involved the 632 km-long line, 23GSWA-SW1, spanning from Cascade to Hamelin Bay along sealed and unsealed gazetted roads. Data collection began on 17/9/23 and concluded on 30/10/23. A segment near Nyabing underwent reacquisition from 3/2/24 to 4/2/24 due to wind noise. The eastern end of the line overlaps with the line 12GA-AF2 from a previous deep crustal vintage.

Data was recorded using Quantum 5Hz geophone receiver nodes positioned at 10m intervals, extending up to 30km from the source (nominal ±8km). Three 60,000 lb Vibroseis source vehicles generated seismic energy at 40m intervals with a 24-second sweep from 3 - 96Hz.

Data processing commenced in November 2023. A custom workflow was developed, specifically tailored to the acquisition parameters, survey objectives, and current geological understanding. Following a thorough initial data quality control (QC) step, a comprehensive first-break picking program was implemented to precisely define the first arrival wavefront. To enhance the depth penetration of the resulting refraction tomography velocity model, the contracted maximum offset for first-break picking was extended from 1,500 meters to 3 kilometres.

Data preprocessing addressed noise sources, primarily traffic-related, through attenuation techniques and signal enhancement. Static corrections were applied using a final datum of 410 meters and a replacement velocity of 5,800 meters per second. Velocity analysis was conducted iteratively before implementing the final Kirchoff Pre-Stack Time Migration (PreSTM). The migrated gathers underwent further conditioning and were stacked to generate two final subsurface images focused on shallow and deep targets, respectively. These images revealed notable features along the entire seismic line, including prominent eastward-dipping formations with significant variations observed at the boundaries of the Youanmi Terrane, South West Terrane and Perth Basin.

Three iterations of reflection tomography were undertaken to generate an interval velocity model in depth. For each iteration this involved sparsely migrating the data and picking residual moveout. The updated velocity model was compared against well logs containing full-waveform sonic and density logs. The final Pre-Stack Depth migrated product showed significant uplift at line bends and areas of sharp lateral velocity contrast, particularly near the Darling Scarp and through the Perth Basin.

Some recommendations are made for future seismic surveys.

1. Resampling for Improved Efficiency: The SW-1 seismic line represents a large dataset due to its length, high trace density, long record length, and a fine 2ms sample rate. While the 2ms sample rate was maintained throughout processing, the maximum sweep frequency used was only 96Hz. In such cases, resampling the data to 4ms can significantly improve processing runtimes and reduce disk space requirements by half. This resampling would not degrade the seismic bandwidth or resolution as the highest recoverable frequency content is well below the Nyquist frequency defined by the original 2ms sample rate. Implementing this approach in future surveys with similar acquisition parameters would enhance processing efficiency without compromising data quality.

2. Targeted Infill Shooting: The infill shots acquired on either side of exclusion zones where standard seismic acquisition was not permitted appear to have limited impact on image quality within those gaps. These additional shots could have been more strategically deployed within the Perth Basin. Several lines from different vintages within the basin exhibit consistently lower reflectivity. Future surveys in the Perth Basin might benefit from utilizing infill shots within these specific areas to potentially improve data quality and subsurface imaging.

Contents

LIST OF FIGURES

LIST OF TABLES

1 INTRODUCTION

1.1 BACKGROUND

HiSeis was contracted to acquire and process deep crustal, 2D seismic reflection data on behalf of the Geological Survey of Western Australia (GSWA) in the Southwest and Midwest Regions of Western Australia as part of the Western Australia Exploration Incentive Scheme (EIS). The first 2D line, named 23GSWA-SW1 (Figure 1), covered approximately 630 km of sealed and unsealed gazetted roads starting in Cascade in September 2023 and finishing in Hamelin Bay on 30 November 2023. Surface elevation varies from 405m in the east to sea-level at the western end of the line (Figure 2).

In the east the 23GSWA-SW1 line overlaps with the 12GA-AF2 line from a previous deep crustal vintage. Moving west the line extends over the western Yilgarn Craton, covering the Youanmi Terrane, South West Terrane and the Perth Basin

Seismic data processing was conducted in Perth, Australia by HiSeis between November 2023 and April 2024.

1.2 OBJECTIVES

GSWA identified the following survey objectives.

- Imaging the deep crustal architecture of the survey area.
- Identify the structure, geometry, and relationship between various geological domains.
- Image from the surface to below the Moho.

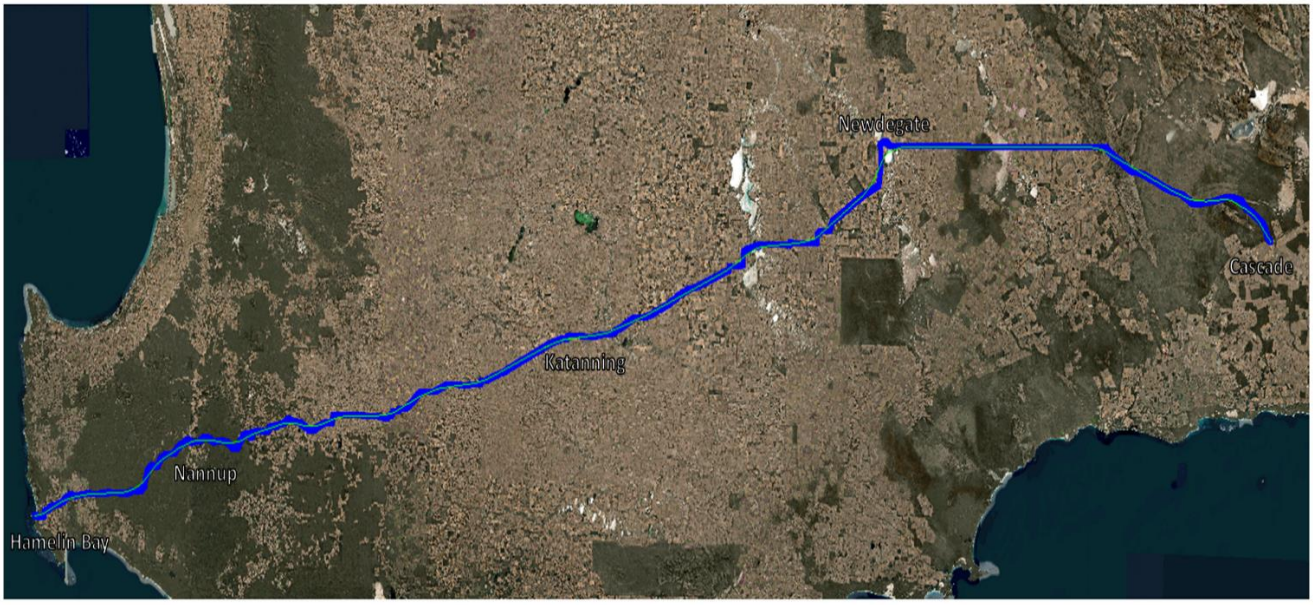

Figure 1. Location map

2 ACQUISITION

Data was recorded using Quantum 5Hz geophone receiver nodes, spaced at 10m intervals along the nominal active split spread of +-8k. However, many more nodes were deployed beyond the nominal spread and all remained active offering maximum offsets out to 27km, resulting in a maximum CDP fold of 440. An inline array of three 60,000 lb Vibroseis source vehicles produced seismic energy, delivering a 24 second sweep through a frequency range of 3 - 96Hz. The nominal source spacing along each line was 40m co-located with receiver stations. Infill/make-up shots were taken at half the nominal source interval when approaching exclusion zones. The source/receiver line is marked blue in Figure 1 above.

Detailed acquisition parameters are presented in Table 1. The Vibroseis sweep definition is outlined in Table 2. A map of source and receiver elevation are shown in Figure 2.

Elevated levels of wind noise were reported during 2 days of shooting near the town of Nyabing between 1/10/23 and 2/10/23**.** Initially it was decided to proceed with acquisition on these days. However, after review in processing a decision was made to reacquire the data for these days. The reacquired data positioned receivers in the same locations as the original acquisition, but with source stations offset by 20m resulting in a double density patch between stations 39711 and 40383. The resulting shot gathers proved to have a much stronger signal to noise ratio. The original shots we retained along with the required data resulting in a higher fold of 880 in this area.

Table 1. SW1 acquisition parameters

2D Acquisition Parameters	
Total Survey Length	1 line, 632km
Receiver Type	Quantum PS-5GR 5Hz geophone
Number of Receiver Stations	63088
Active Receiver Spread (maximum)	Nominal +- 8km split spread, all live with additional receivers being deployed and retrieved.
Receiver station spacing	10m
Total Number of Source Stations	15951, plus 1055 reacquired.
Source Station Spacing	40m nominal with 20m infill around gaps
Max Fold	440 using all offset, 880 in reacquired area
Offset	+-8000m nominal, 27000m max
Record length	20sec
Sample interval	2ms
Coordinate reference system	GDA2020, MGA Zone 50

Table 2: SW1 sweep parameters.

Standard Sweep Definition SW1	
Vibrators	INOVA AHV-IV 60, 000 lb
Electronics	INOVA VibPro HD
Sweep Frequency Range	3 – 96 Hz
Sweep Duration	24 second nominal
Sweep Type	Weibull base
Tapers	500ms in, 600ms out
Vibrator Array	3 vibrators inline configuration
Operating Force	70%
Phase Locking	Ground force
Amplitude Control	Peak-to-peak

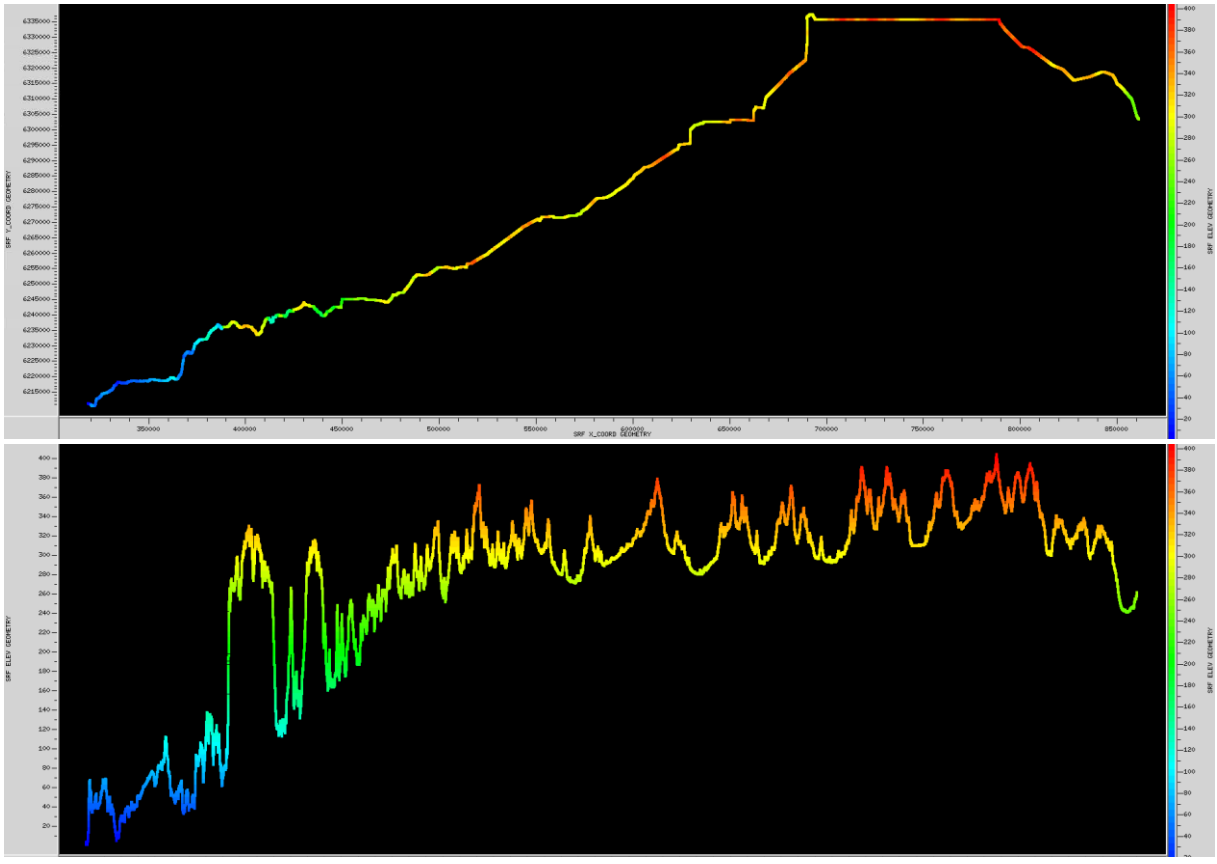

Figure 2. Elevation map and profile

In Figure 2 (above) the top image shows the receiver X and Y coordinate with the 2D line coloured by elevation. The bottom image shows the elevation profile with the receiver position on the X-axis and elevation on the Y-axis.

Below in Figure 3 the fold of the survey is shown using the CDP X and Y coordinates and the 2D line coloured by fold. The fold map includes all active receivers and the reacquired portion of data around Nyabing. Nominal fold is around 400, while the reacquired portion shows a double nominal fold around 800.

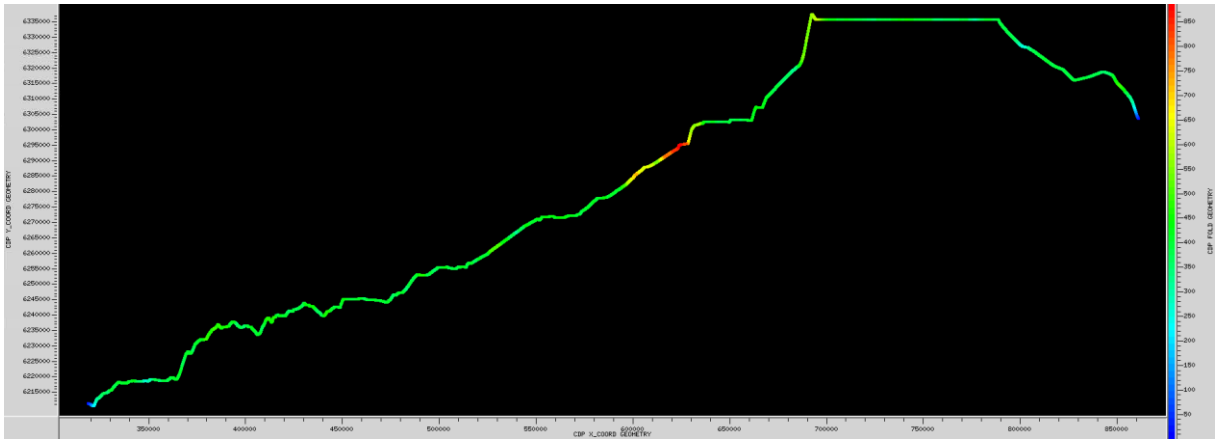

Figure 3. CDP Fold map

3 PROCESSING

3.1 OVERVIEW

The processing flow included refraction tomography, comprehensive pre-processing and noise attenuation processes, several iterations of velocity analysis and Pre-stack Time Migration. The pre-processed gathers were also used to perform 3 iterations of reflection tomography to update the velocity model prior to producing a final Pre-stack Depth Migrated product as explained in section 4.

A final datum of 410m and replacement velocity of 5800m/s was selected for the Pre-Stack Time Migration flow so all data would lie below the final datum and the data would tie with the adjacent 12GA-AF2 vintage. Pre-Stack Depth Migration was run from topography.

Testing was generally performed on a subset of shot gathers evenly spaced along the line with an interval of 5000 stations. However, at locations such as the Darling Scarp and Perth Basin a denser QC was undertaken as required. Results from testing were presented during weekly meetings with GSWA for production approval. Presentations from weekly meetings are listed in appendix 8.4**.**

Table 3. Processed data parameters

Processed data parameters	
Processed record length	PreSTM: 20sec/50km and 8sec/26km PreSDM: 50km
Processed sample rate	Time:2ms Depth: 4m
Final datum	410 m
Replacement velocity	5800 m/s
Coordinate reference system	GDA 2020, MGA zone 50
Polarity	As acquired
Phase	Zero phase

3.2 PROCESSING FLOW

Table 4. 2D processing flow.

2D Processing Flow
1. SEGY input: 20000ms @ 2ms
2. Geometry assignment: CDP spacing of 5m Offset binning 50m – 10050m (100m) Manual picking of CDP track close to receiver line
3. First break picking of every shot out to 3km offset

4. Refraction tomography & refraction static computation
   Final datum 410m, replacement velocity 5800 m/s
5. Quality control of the refraction static solution (on shot records, every 100th shot)
6. Trace kill dead/weak traces
7. Amplitude balance: $T^{1.1}$ and $Offset^{1.1}$, wrapped around processes 8 to 13 as required.
8. TFDN common channel domain: 3-250HZ, 11 traces, 250ms
9. Apply refraction statics to floating datum
10. Deconvolution:
    Zero phase spike,
    1.5s window, 100ms operator, 1% pre-whitening
11. Air blast attenuation: 345 m/s
12. Surface wave noise attenuation: 100ms wrap-around AGC
    Hard rock: 2800m/s, 3-80Hz
    Basin: 1500m/s, 3-80Hz
13. TFDN shot domain: 10-250HZ, 7 traces, 500ms
14. Constant velocity stack analysis for velocity guide function
15. 1st pass residual statics:
    4sec window centred on 3000ms
    11 CDP smash to form pilot trace
16. 1st Pass IVA on conditioned, pre-migration, super-gathers at 5km intervals.
17. 2nd pass residual statics:
    2sec window centred on 3000ms in hard rock and picked horizon in Perth Basin
    11 CDP smash to form pilot trace
18. Pre-Stack Time Migration for velocity analysis:
    0-8000ms @4ms
    Every 5th CDP
    Offset binning 50m - 8050m x 100m
    75deg dip limit, 30km aperture
19. 2nd pass IVA picked at 2km intervals
20. Pre-Stack Time Migration for velocity analysis:
    0-20000ms @ 4ms
    Every 5th CDP
    Offset binning 50m - 8050m x 100m
    75deg dip limit, 30km aperture
21. 3rd pass IVA picked at 1km intervals.
22. Amplitude recovery for final migration: 4000ms AGC and, remove $T^{1.1}$
23. Shift to final datum 410m
24. Final PreSTM:
    0-20000ms @ 2ms
    5m CMP spacing,
    Offset binning 50m-10050m x 100m,
    75deg dip limit, 30km aperture

25. Linear noise attenuation: 100ms wrap-around AGC
    5000m/s dip
    100m trace spacing.
    0-120 Hz

26. High density velocity analysis: QC at 500m intervals and pick as required.

27. Post migration amplitude balance:
    8 second dataset: 500ms AGC
    20 second dataset: 3000ms AGC

28. Trace mute:
    8 second dataset: Near 0-15 degrees
    Mid 15-30 degrees
    Far 30-45 degrees
    Full hand-picked (50deg approx.)

    20 second dataset: 2deg inner, hand-picked outer

29. Stack using 1/n

30. Random noise attenuation: F-X deconvolution
    15 traces
    10% white noise
    750ms window
    0-250 Hz

31. Time-varying bandpass filter
    10-16-80-100, 0-300ms
    8-12-80-100, 400-800ms
    5-10-60-80, 1200-5500ms
    4-8-60-70, 6500-9000ms
    4-8-40-60, 11000-14500ms
    4-8-40-50, 15500-20000ms

32. Coherence filter:
    8 second dataset: 11 traces
    ±9ms/trace

    20 second dataset: 21 traces
    ±9ms/trace

33. Time-varying gain: 8 second dataset only, -8dB/s @ 0-1000ms

34. Post-stack amplitude balance: record length AGC

35. Time/depth conversion using smoothed migration velocity

36. Output data to SEGY

3.3 DATA PREPARATION & QC

Data quality was monitored daily during acquisition with ongoing uploads of receiver gathers from the field to the office for visual inspection and geometry QC. Upon completion of acquisition shot gathers were transcribed in SEGY format and returned to the Perth office along with the observer logs and survey information further QC and processing.

Shot and receiver peg coordinates and relational information data were cross-checked throughout loading and geometry assignment. The geometry was verified by overlaying a theoretical airwave and refractor velocities on the raw data. Figure 4 shows the header overlay for shot QC performed on the 4/10/23.

Noise QC plots were generated during field QC as seen in Figure 5. These plots are derived using the signal-to-noise ratio over a window. Typical sources of noise were vehicle travelling on the road, stationary infrastructure, and wind.

Elevation measurements were compared between source stations and the surveyed receiver stations. Some discrepancies in the recorded source elevations were observed. Given the near coincident source and receiver positions, these discrepancies were corrected using a bulk shift to align with the receiver elevations.

Rigorous first break picking was carried out using a combination of manual and automated picking methods for every record. HiSeis was contracted to pick first breaks out to a maximum offset of 1500m. However, given the high data quality and ease of picking HiSeis extended the picking out to 3km to provide a better velocity model from refraction tomography and a better refraction statics solution.

Data was binned with a nominal 5m trace spacing. Given the crookedness of the line, the crossline offset of the CDP track was significant and would cause gaps and artefacts in the stack data. To minimise these gaps and artefacts a CDP track was manually picked following closer to the receiver line and a 51-point smoother was applied. Offset binning was performed using 50m – 10050m x 100m.

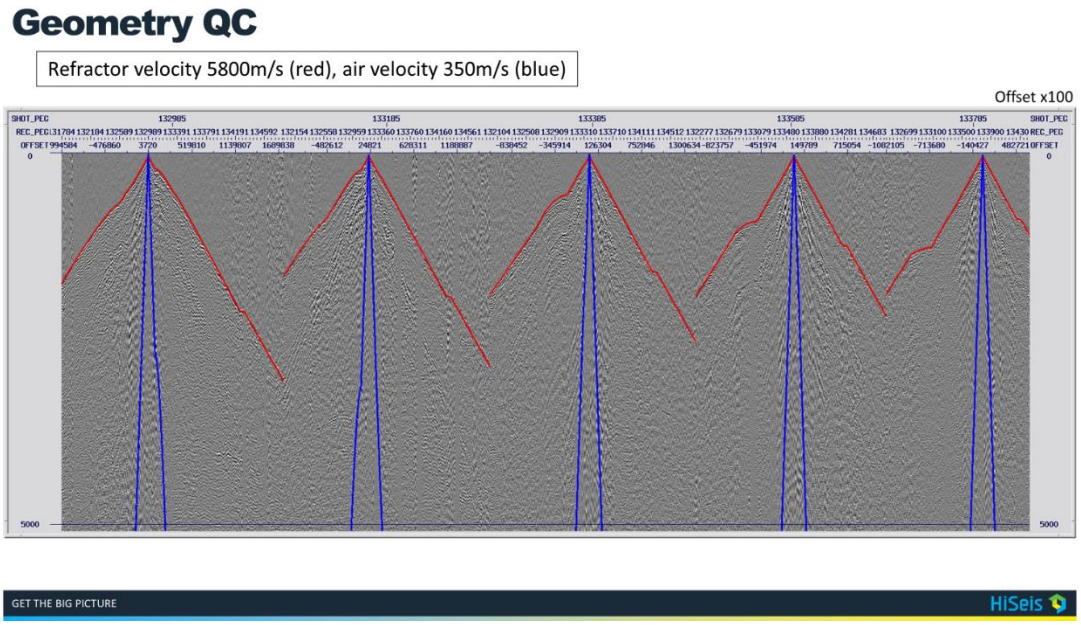

Figure 4. 2D Line raw shot gather air blast (blue), refractor (red)

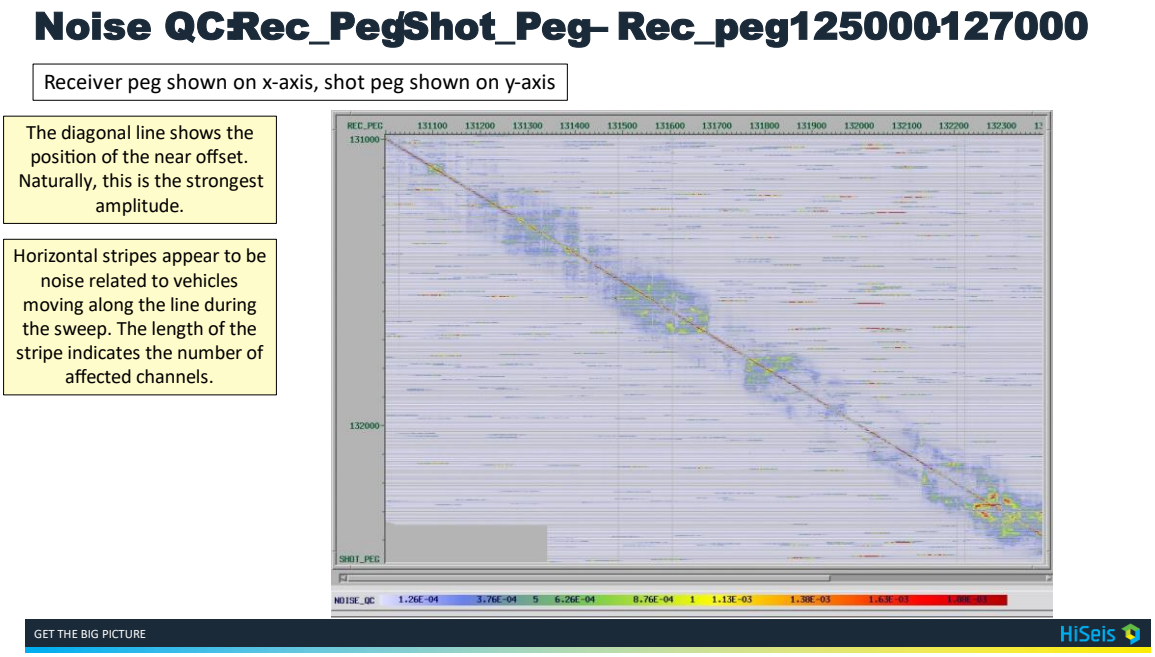

Figure 5. Example noise QC plot

3.4 REFRACTION TOMOGRAPHY

Rigorous first break picking and high-resolution refraction tomography was used to generate a velocity model, ray-path model and extracted iso-velocity surfaces. These attributes provide excellent near-surface geological information and may be used to determine the depth to the top of fresh rock as well as identify any features that may imprint on this contact. The velocity model may also be used in the calculation of refraction statics.

The refraction tomography inversion process ray traces synthetic travel times for each shot such that the difference between the input first breaks picks and synthetic first breaks are minimised. By comparing estimated and known travel times, the velocity of the medium through which the rays travelled can be iteratively deduced. As the computation is based on refracted energy, the model is accurate to the top of the deepest refractor where adequate ray coverage exists.

The velocity model for 23GSWA-SW1 (Figure 6) appears well defined with strong ray penetration through the weathering layers over the Yilgarn and South West Terrane. In the Perth Basin the shallow velocity is defined to ~2km. However, the depth to basement cannot be determined as rays (Figure 7) do not appear to penetrate deep enough with the 3km absolute offset first break picking limit.

Due to the length of the line please note the very large vertical exaggeration on Figure 6, Figure 7 and Figure 8 below.

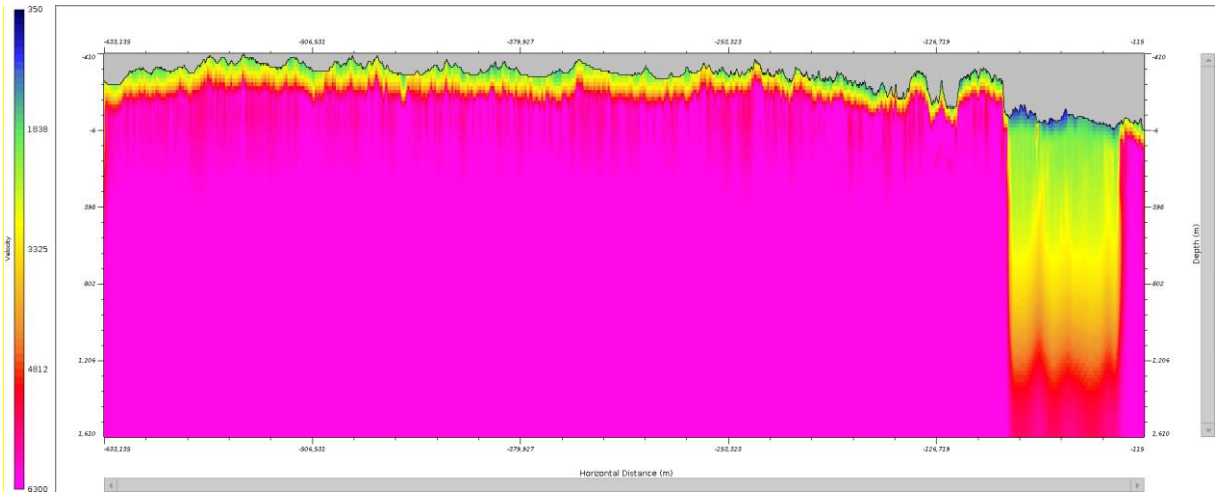

Figure 6: Refraction tomography velocity model. East (left), West (right).

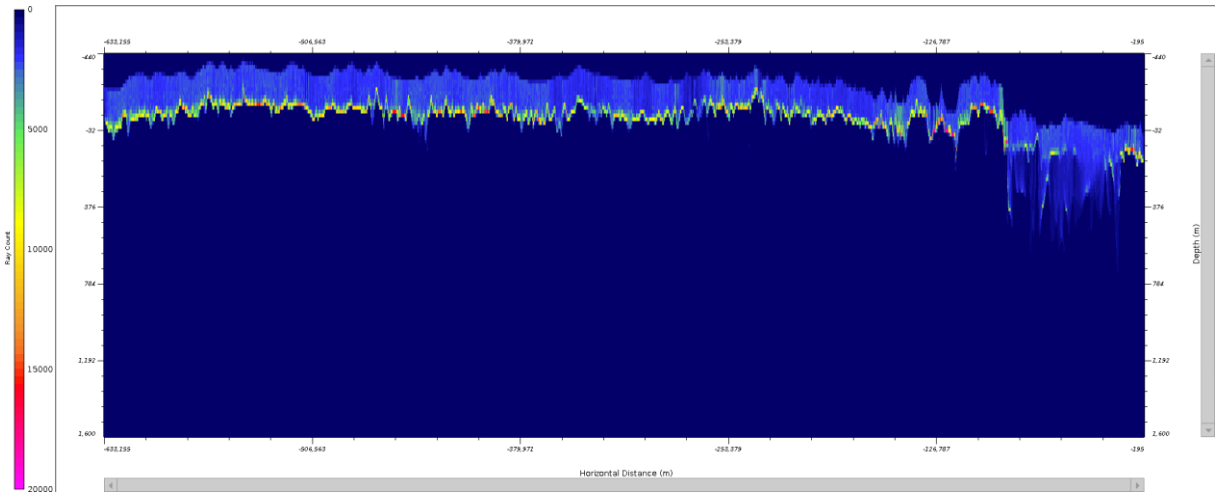

Figure 7. Refraction tomography ray tracing model. East (left), West (right).

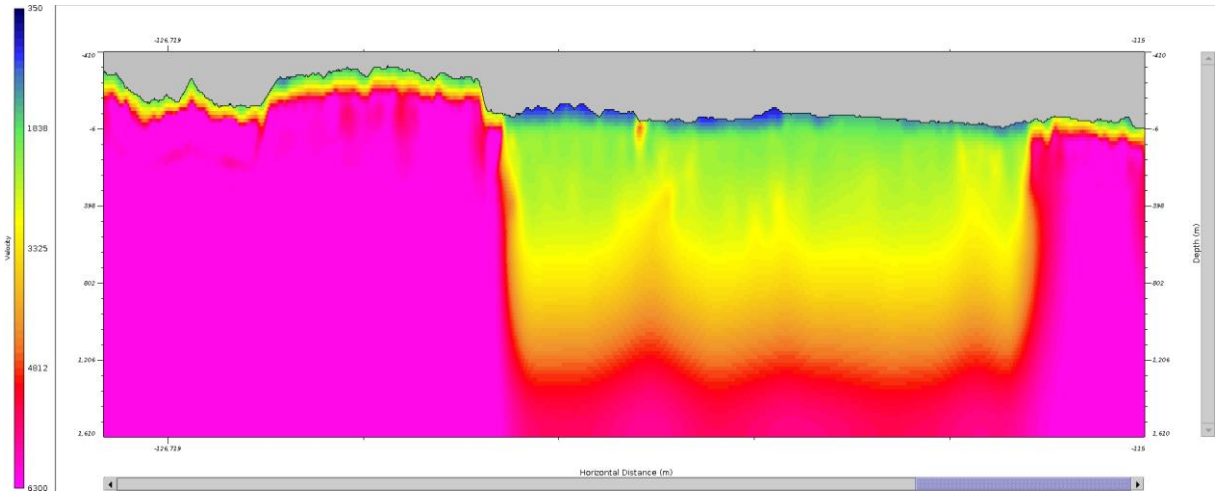

Figure 8. Refraction tomography velocity, Perth Basin. Shallow velocity anomaly aligns with Bunbury basalt. East (left), West (right).

3.5 PRE-PROCESSING

At the completion of first break picking and refraction tomography, data was imported to the processing software. The pre-processing workflow included several processes designed to remove noise, enhance signal, and prepare the data for migration. Where required the data was wrapped in a temporarily applied gain of T^1.1 and offset^1.1.

3.5.1 Vehicle noise attenuation

Vehicles were a strong source of noise throughout the survey. Given the length of the active spread and shot intervals between sweeps it was not feasible to halt traffic during recording. During a sweep, vehicles travelling along the spread pass several receivers. On the subsequent sweep those vehicles are moving past a different set of receivers. By sorting the data into common receiver domain, small

groups of noise affected traces are positioned next to clean data. Using this sorting a time-frequency denoise (TFDN) process can be used to attenuate the noise on the affected traces. Figure 9 below shows example shots before vehicle noise attenuation. Figure 10 show the noise attenuation applied in common receiver domain and sorted back to shot domain.

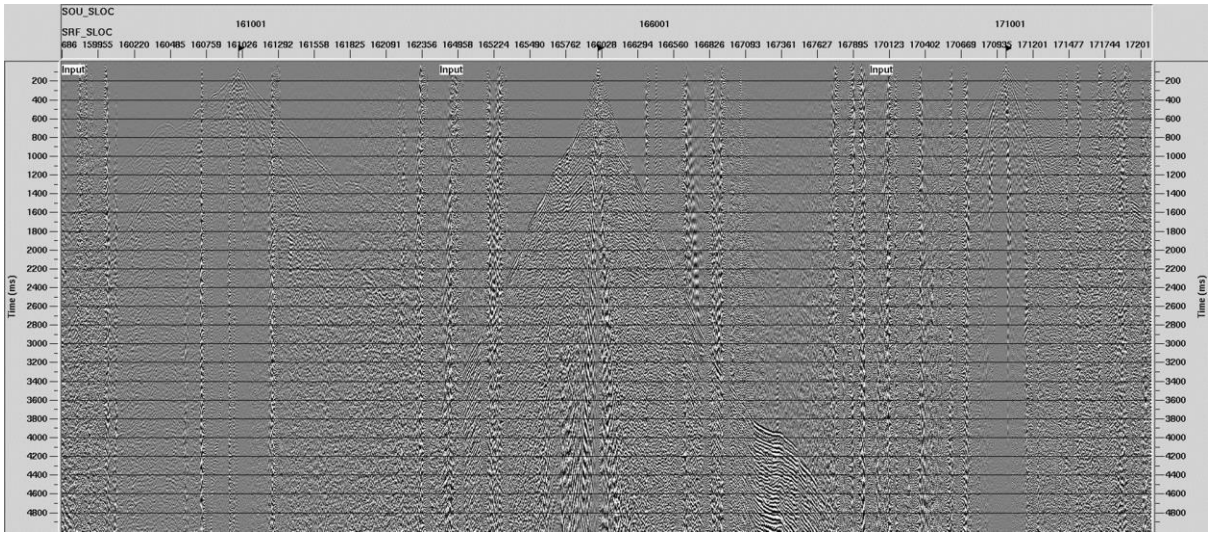

Figure 9. Input to vehicle noise attenuation.

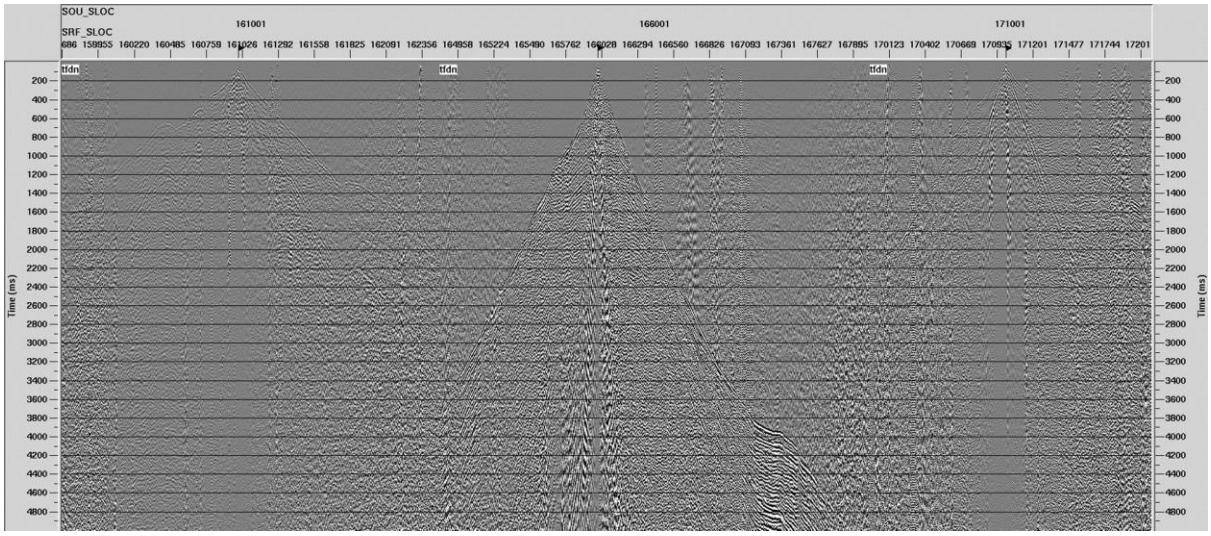

Figure 10. Vehicle noise attenuation applied.

3.5.2 Refraction Statics

Statics are corrections applied to seismic data to compensate for the effects of variations in elevation, near-surface low-velocity-layer (weathering) thickness, weathering velocity, and/or to shift data to a reference datum. In this workflow the refraction statics were applied prior to air blast attenuation and zero-phase spike deconvolution and surface wave noise attenuation. This allows for better noise attenuation as surface waves become more linear once statics are applied.

Refraction statics were calculated using the mean CDP delay time algorithm and compared against statics calculated in refraction tomography. Application of statics proceeded using results from the mean CDP delay time method. First break picks with an offset range greater than 150m were used in the calculation. A 5800m/s replacement velocity and final datum elevation of 410m were used to calculated static shifts to the floating datum for processing. Figure 11 and Figure 12 show the source and receiver static to final datum respectively.

The chosen replacement velocity of 5800m/s is not ideal for the Perth Basin as the refractor in the basin is in fact much slower (around 2100m/s). However, the vast majority of the line is over a hard rock environment, and the chosen velocity and datum tie with the adjoining 12GA-AF2 line. Imaging in the basin does appears slightly degraded from the use of this replacement velocity. However, depth migration, as explained in section 4, was performed from topography removing the assumption of replacement velocity and final datum.

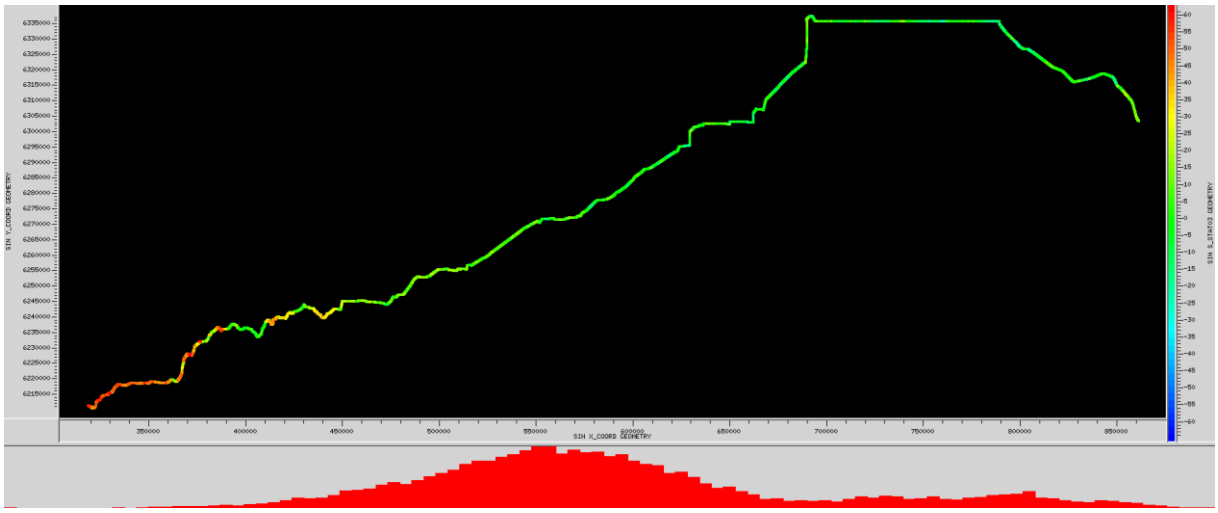

Figure 11. Source refraction static to final datum.

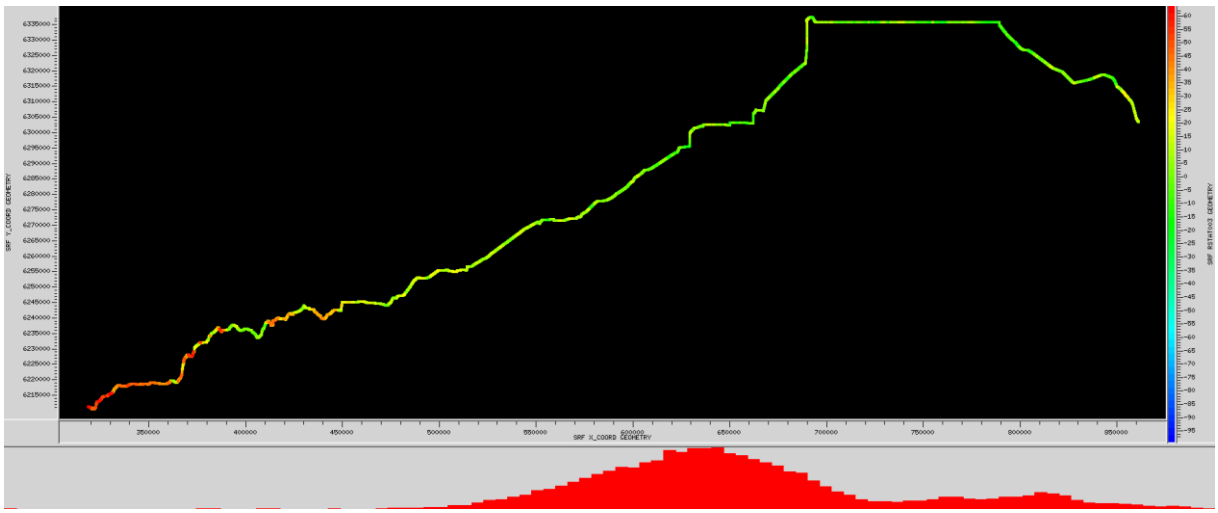

Figure 12. Receiver refraction static to final datum

3.5.3 Deconvolution

The recorded seismic signal may be considered as a convolution of the source signal with the instruments, geophones, and earth response. This signal often includes undesirable effects such as reverberation, attenuation and ghosting that mask the primary reflection (Robinson et al, 2008). Deconvolution aims to remove these effects, whitening the spectrum and increasing temporal resolution.

A zero-phase spike deconvolution using a 100ms operator length was applied to the data as seen in Figure 13 and Figure 14. The resulting data is zero-phase with a flatter, more broadband amplitude spectrum. The whitening of the frequency-amplitude spectrum, Figure 14 inset, gives the appearance of attenuating the high amplitude, low frequency noise associated with ground roll.

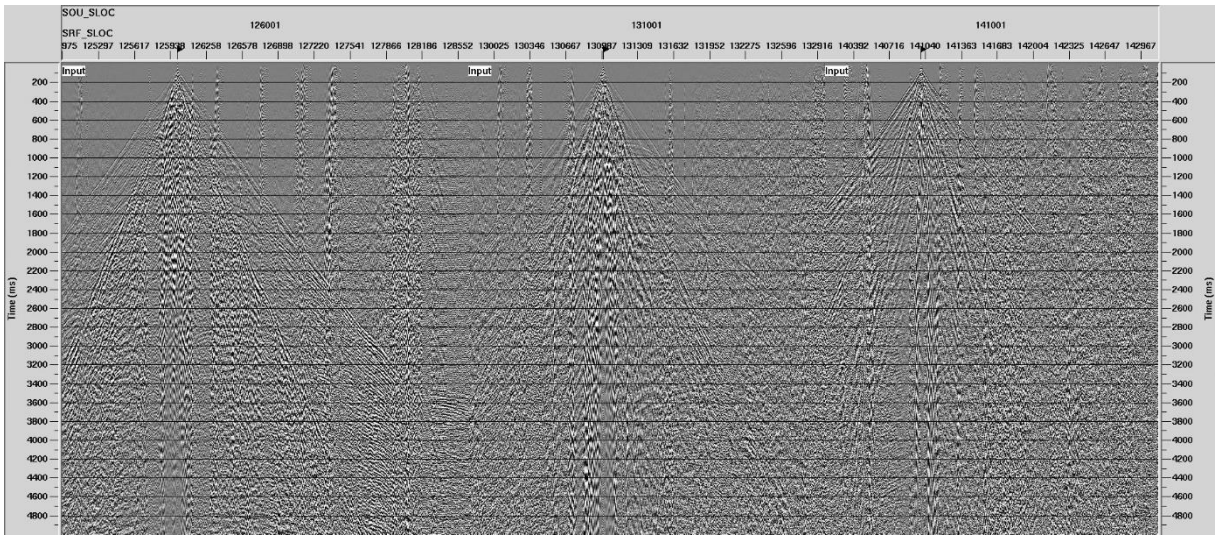

Figure 13. Data prior to zero-phase spike deconvolution

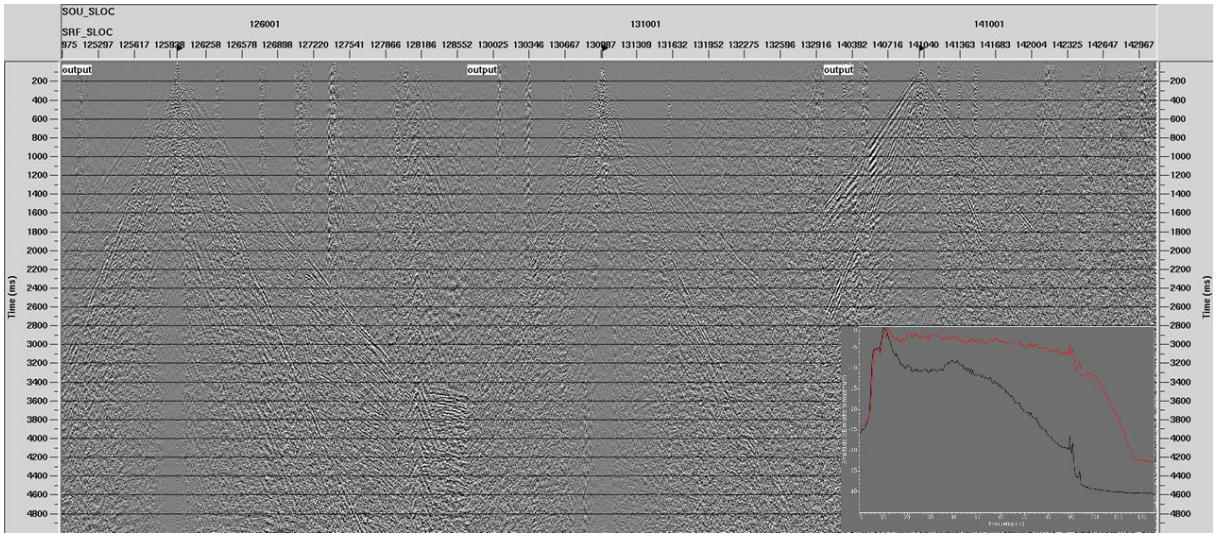

Figure 14. Zero-phase spike deconvolution applied.

3.5.4 Airblast Attenuation

Air blast attenuation was applied using a velocity of 345m/s. The process operates trace by trace, searching for anomalous amplitudes over a window centred on the theoretical two-way-time calculated from the defined velocity. The effect of air blast attenuation can be observed in the images of cumulative noise attenuation shown in Figure 15 and Figure 16.

3.5.5 Surface wave noise attenuation

The strongest noise type in land seismic is typically the ground roll energy. It is comprised of surface waves / Rayleigh waves which are characterised by broad bandwidth, high amplitude, and a low velocity.

Surface wave noise attenuation (SWNA) was performed in shot domain wrapped within an 100ms AGC. Two seismic domains were identified, the craton and the basin, which contained surface waves propagating at different velocities. In the craton area a target velocity of 2800m/s was used, and in the basin area 1500m/s was used. The effect of SWNA can be observed in the images of cumulative noise attenuation shown in Figure 15 and Figure 16.

3.5.6 Despike TFDN

Spikes remaining in the data after the above processes may be attenuated using a secondary pass of time-frequency denoise (TFDN) in the shot domain. TFDN despike was performed in shot domain using a 7-trace window, over frequencies from 10 Hz to 250 Hz and temporal widow of 500ms.

Data was then passed through a statistical analysis where an RMS amplitude was calculated over 2 windows. The absolute amplitude and RMS ratio between windows were used compared against a threshold value and traces outside of that threshold were killed. The effect of TFDN can be observed in the images of cumulative noise attenuation shown in Figure 15 and Figure 16.

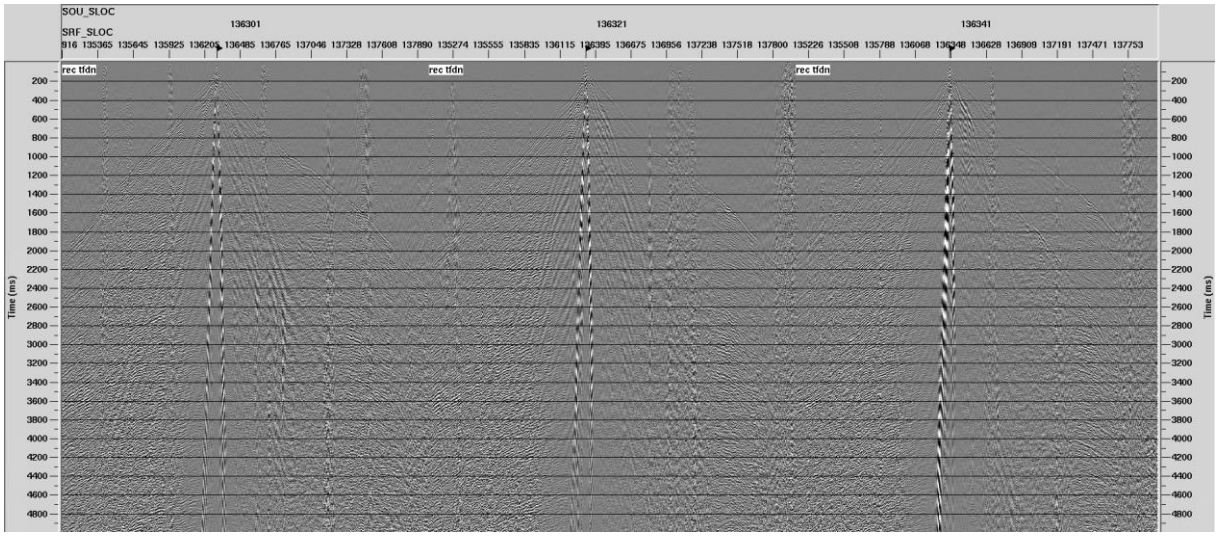

Figure 15. Input to noise attenuation.

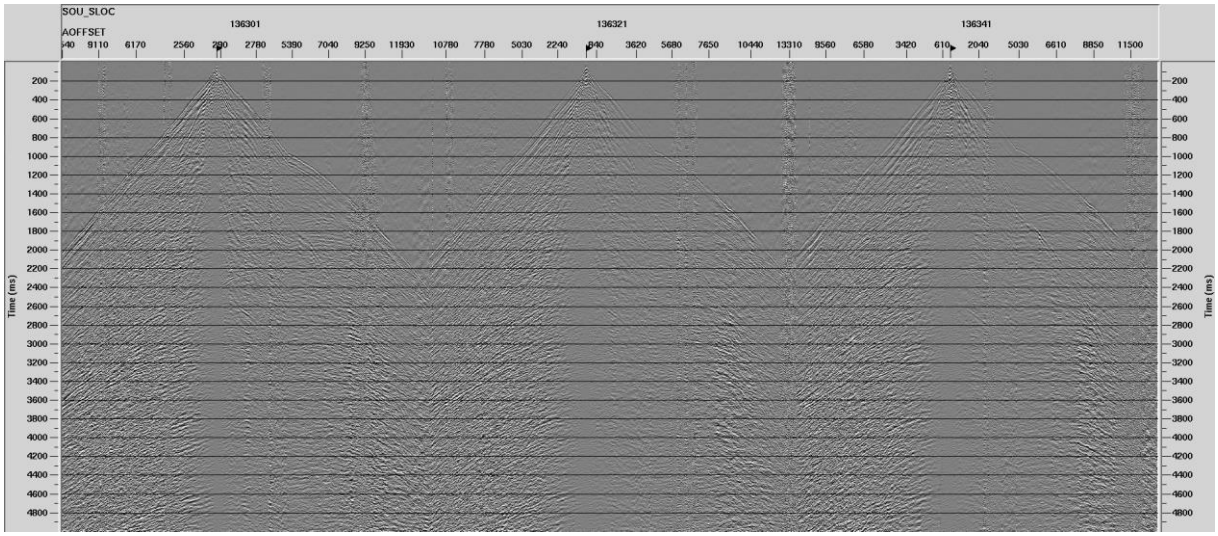

Figure 16. Decon, Air blast, SWNA, TFDN applied.

3.5.7 Residual statics

Residual statics were computed in 2 passes. The first pass used the initial velocity model for NMO correction. After the 1st pass IVA model (see section 3.6.2) became available a second pass of residual statics was computed providing a superior result.

Noise attenuated shots were sorted to CDP gathers and NMO corrected. Data were conditioned with an AGC, linear noise attenuation and bandpass filter. An 11 CDP smash was used to generate pilot traces. The 1st pass of residual statics used a flat 4 second window centred on 3 seconds. The 2nd pass of residuals used a 2000ms window centred on 3000ms in hard rock combined with a picked horizon following the shape of the Perth Basin.

3.5.8 Amplitude scaling

Variations in amplitude can be caused by differences in source or receiver coupling, noise, or differences in near surface conditions which affect attenuation. Two observations were made relating to amplitude scaling along the SW1 line. Firstly, there was significant vehicle noise which varied in intensity along the line. Secondly the line transitions from hard rock in the east to sedimentary basin in the west which exhibits higher than expected levels of attenuation.

Following noise attenuation, Surface Consistent Amplitude Compensation (SCAC) was tested using source, receiver and offset terms. The SCAC test was migrated and compared with data which used a 4000ms AGC and removal of $T^{1.1}$ prior to migration. SCAC provided inconsistent results along the line, whereas the AGC method appeared more robust. The long window used in this method partially preserves the amplitudes while accounting for noise and absorption. After careful consideration processing proceeded using the AGC method.

3.6 VELOCITY ANALYSIS

A critical step in seismic processing is Interactive Velocity Analysis (IVA). The velocity defined through IVA is used to NMO correct the gathers for stacking, residual statics calculation and in the final migration. For this project, after defining the initial velocity model using constant velocity stacks, 3 iterations of IVA were performed.

3.6.1 Initial velocity model

The initial velocity model was derived from constant velocity stacks (CVS) where a suite of stacks are produced using a single velocity function. From the reflectivity apparent in these stacks a time and spatially varying velocity can be coarsely defined forming the initial velocity model. This initial velocity model was used in the production of noise attenuation QC stacks and the 1st pass of residual statics.

3.6.2 1st pass IVA

Noise attenuated shots were sorted to CDP gathers and NMO corrected using the initial velocity model. Gathers were conditioned before producing super-gathers at a 5km interval. Interactive velocity analysis was used to define a velocity model down to 8 seconds.

Figure 17 shows the first pass IVA from the hard-rock craton area. As expected, the velocity trend is much faster than that of the Perth Basin shown in Figure 18.

The resulting velocity model was then used in the computation of the 2nd iteration of residual statics as described in 3.5.7 Residual statics.

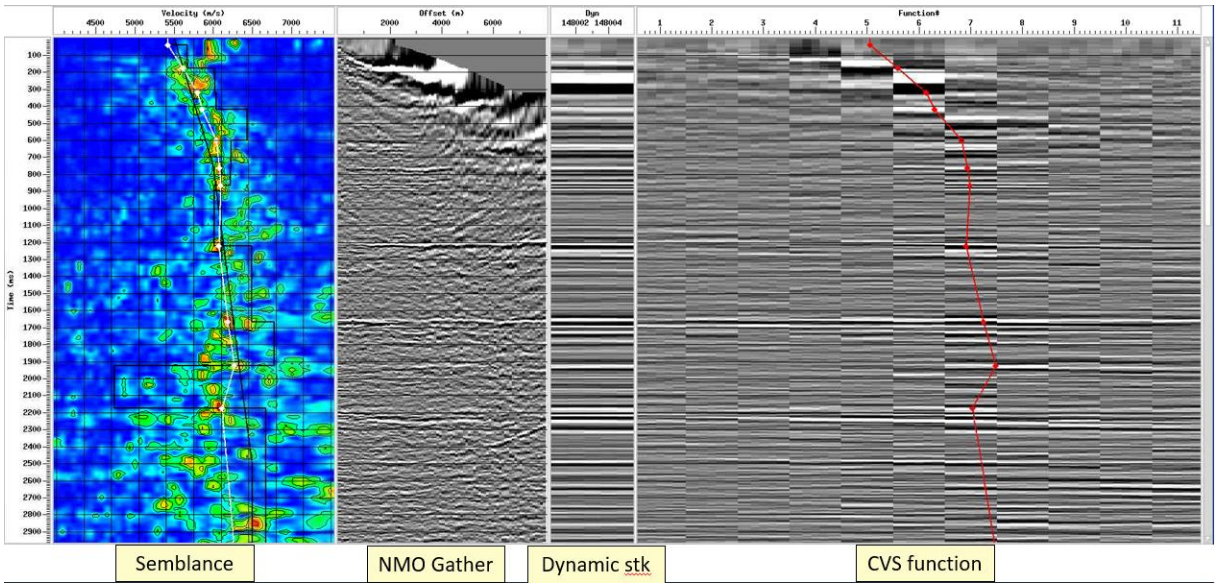

Figure 17. Interactive Velocity Analysis (IVA) from craton area.

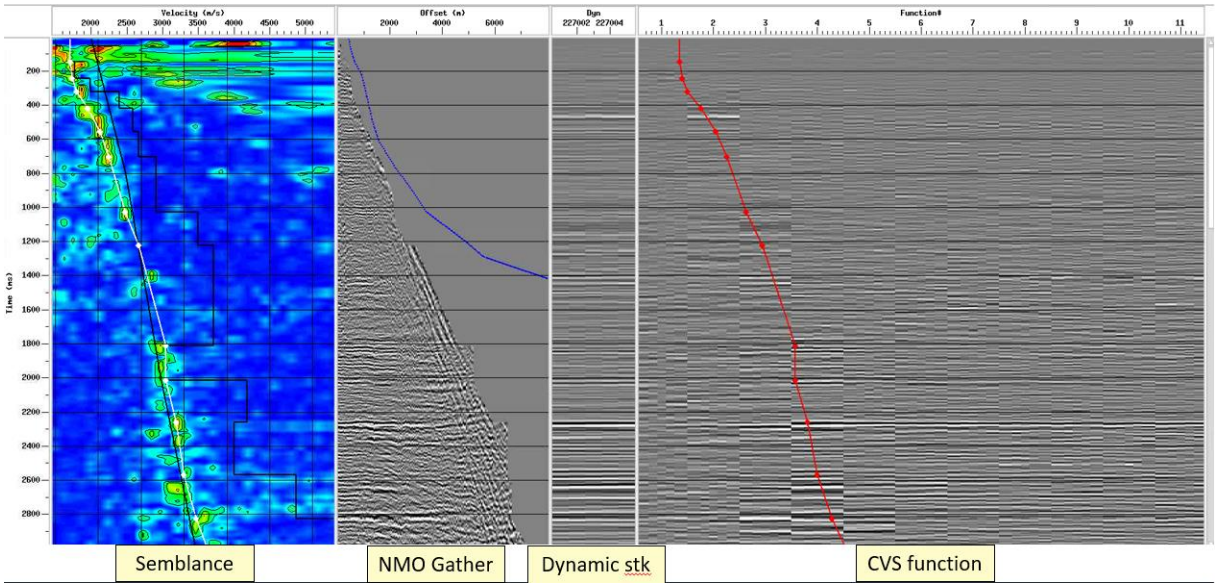

Figure 18. Interactive Velocity Analysis (IVA) from Perth Basin.

3.6.3 2nd pass IVA

The noise attenuated data had 2nd pass residual statics applied and was shifted to final datum before migration of every 5th CDP using the 1st pass IVA velocity. The second pass of IVA was then performed using the migrated gathers, picking at an interval of 2km.

3.6.4 3rd pass IVA

The noise attenuated data had 2nd pass residual statics applied and was shifted to final data before migration of every 5th CDP using the 2nd pass IVA velocity. The third pass of IVA was then performed using the migrated gathers, with a focus on picking the Perth Basin at an interval of 1km.

This 3rd pass velocity, shown in Figure 19, was used in the in the final Pre-stack Time Migration. A heavily smoothed version of this velocity was also used in the time-depth conversion as explained in section 3.9.

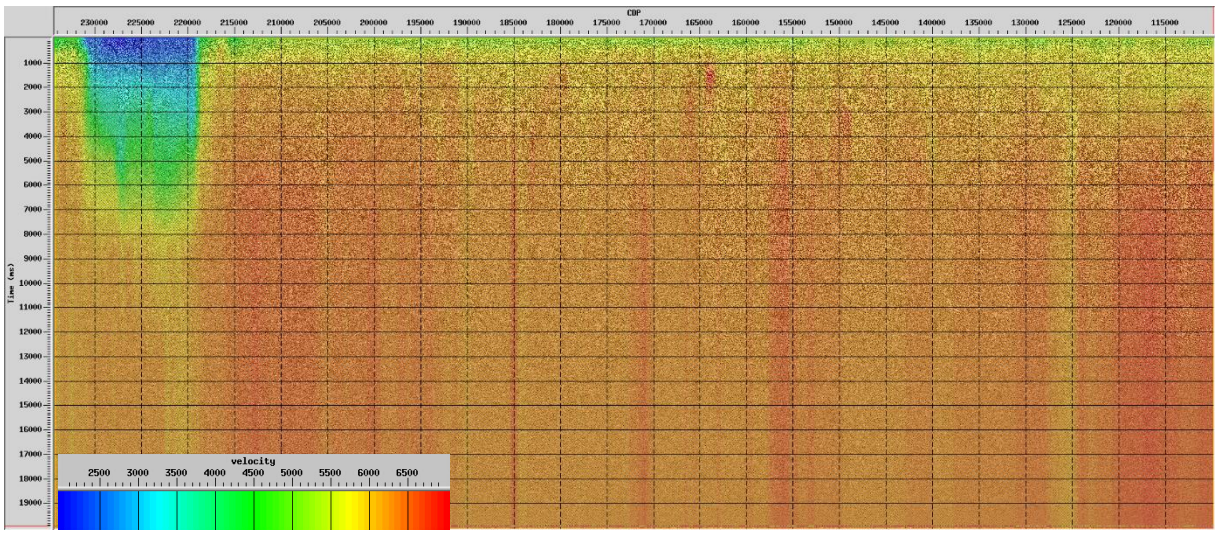

Figure 19. Final PreSTM RMS velocity overlain on the non-migrated stack.

3.7 KIRCHHOFF PRESTM

The Kirchhoff Pre-stack Time Migration (K-PreSTM) algorithm is suited to imaging moderately complex geologies with a gradually varying velocity field. K-PreSTM produces seismic images in terms of travel-time rather than depth and must then be converted using a velocity model to approximate depth. Prior to final migration a suite of tests were performed to determine the optimal migration aperture and dip limit.

K-PreSTM was performed from final datum (410 m), using an output CMP spacing of 5m and offset binning of 50m-10050m x 25m. A 15km half-aperture was used with a 75deg dip limit. This larger than typical migration aperture takes advantage of the long offsets beyond the minimum 8km offset with the aim of imaging deeper events.

3.8 POST MIGRATION PROCESSING

3.8.1 Gather conditioning

Linear noise attenuation was applied to migrated gathers targeting steeply dipping events with a velocity of 5000m/s.

A post-migration amplitude balance was performed tailored to each of the 8 second and 20second record length datasets. For the 8 second dataset a 500ms AGC was used, which helps to enhance the shallow features of the dataset. On the 20 second dataset a 3000ms AGC was applied, balancing the amplitudes but without damaging contrast of deeper events such as the Moho.

3.8.2 High-density velocity analysis (HDVA)

Following noise attenuation a high-density velocity analysis HDVA was undertaken. Gathers were reviewed at 500m intervals, and where necessary the velocity model was adjusted to correct any excessive moveout. The migration velocity was removed from the gathers and the HDVA velocity was applied.

3.8.3 Trace muting

Inner and outer mutes applied to the migrated gathers change the contribution of different offsets to the stacked image. For gathers limited to 8 seconds, angle mutes as, explained in Table 5, were used to produce near, mid, far, and full stacks.

When applying angle mutes the record length is typically truncated as a result. Hence angle mutes were not applied when producing the stack with a 20 second record length. For this product only a 2-degree inner mute was applied along with the hand-picked outer mute.

Table 5. Mute parameters

8 second data mute parameters	
Near	0 – 15 degrees
Mid	15 – 30 degrees
Far	30 – 45 degrees
Full	0 – hand-picked outer

3.8.4 Stacking

Stacking was performed using a 1/n normalisation where n is the number of samples being summed. The number of samples can be raised to a power, in this case the exponent used is 0.5.

The stack output at this point is referred to as the raw stack.

3.8.5 Post-stack conditioning

Post-stack conditioning included random noise attenuation, time-varying bandpass filtering, coherence filtering and time-varying gain. To attenuate random noise an F-X deconvolution process was applied. This used a 15-trace window, 10% white noise and a 750ms temporal window.

As the signal is returned from the earth higher frequencies are attenuated more rapidly with depth. As a result, a time-varying bandpass filter can be employed to remove noise at frequencies above what is expected for signals at depth. The filter was applied using the parameters in Table 6 below. The filters are linearly interpolated between the defined points.

Table 6. Time-varying bandpass filter

Filter	Application time
10-16-80-100	0 – 300 ms
8-12-80-100	400 – 800 ms
5-10-60-80	1200 – 5500 ms
4-8-60-70	6500 – 9000 ms
4-8-40-60	11000 – 14500 ms
4-8-40-50	15500 – 20000 ms

A coherence filter was used to enhance the signal by estimating the continuity of events over a spatial window. For the 8 second record length data an 11-trace window was used with a dip limit of 9ms/trace. The 20 second record length data had this filter increased to 21 traces with the aim to improve continuity of deeper events.

With the goal of improving the strength of near surface events and more evenly balancing amplitudes a time-varying gain was applied to the 8 second stack using -8dB/s from 0 to 1000ms.

A record length (single scalar) AGC was applied to each of the 8 second and 20 second stacks. This laterally balances the amplitudes of the stack along the line.

3.9 TIME-DEPTH CONVERSION

The final PreSTM velocity model was smoothed using a 5km smoother. The purpose of smoothing the velocity is to reduce sharp lateral velocity changes that can result in anomalous pull-up and push downs in the depth converted section. Because of the discrepancy between the replacement velocity, 5800m/s and the actual refractor velocity, ~2500m/s, it was necessary to clip the minimum velocity for depth conversion. Several tests were performed to assess the clip value resulting in the selection of a minimum velocity of 2750m/s. This provided an acceptable mistie in depth. However, problems such as this replacement velocity discrepancy and sharp lateral velocity change as seen at the Darling Scarp are best addressed using Pre-Stack depth Migration.

3.10 FINAL PRESTM STACKS

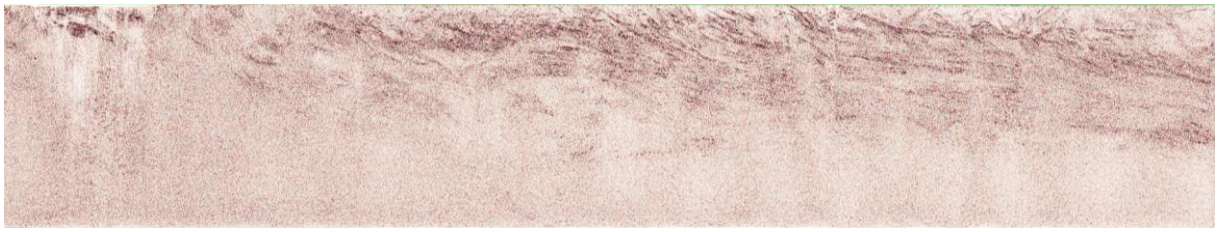

Figure 20. PreSTM Full stack, 20 seconds

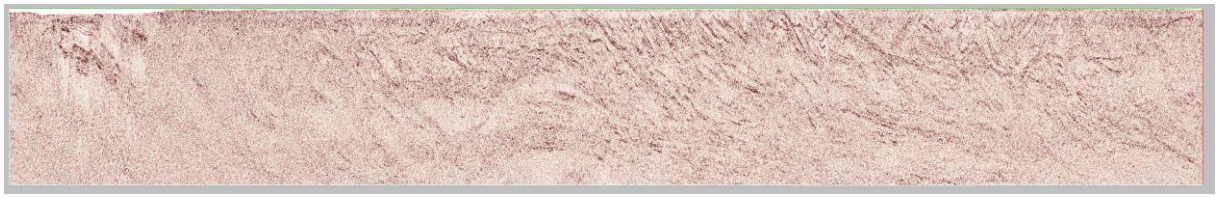

Figure 21. PreSTM Full stack, 8seconds

Figure 22. PreSTM Near stack, 8 seconds

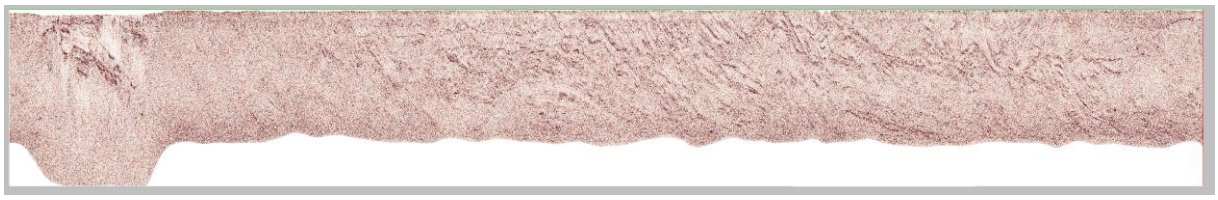

Figure 23. PreSTM Mid stack, 8 seconds

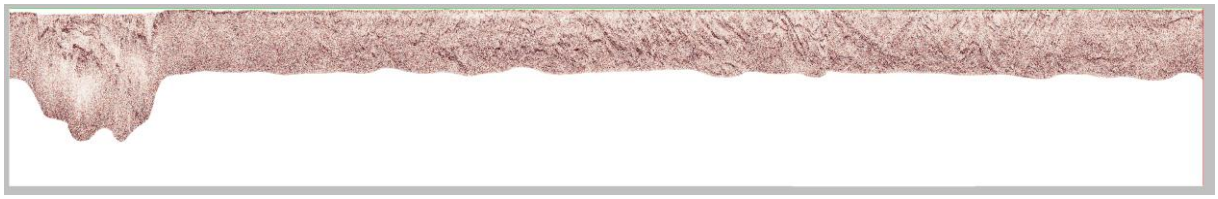

Figure 24. PreSTM

4 DEPTH IMAGING

The imaging algorithm known as Kirchhoff Pre-stack Depth Migration (K-PreSDM) has the potential to address non-hyperbolic moveout resulting from lateral velocity variations, providing accurate depth positioning for seismic images. A depth imaging method proposed by Ziramov et al. (2022) was used, which is uniquely suited to a hard rock environment and utilises both refraction and reflection tomography for velocity model building (VMB).

The depth imaging workflow is illustrated in Figure 25 below.

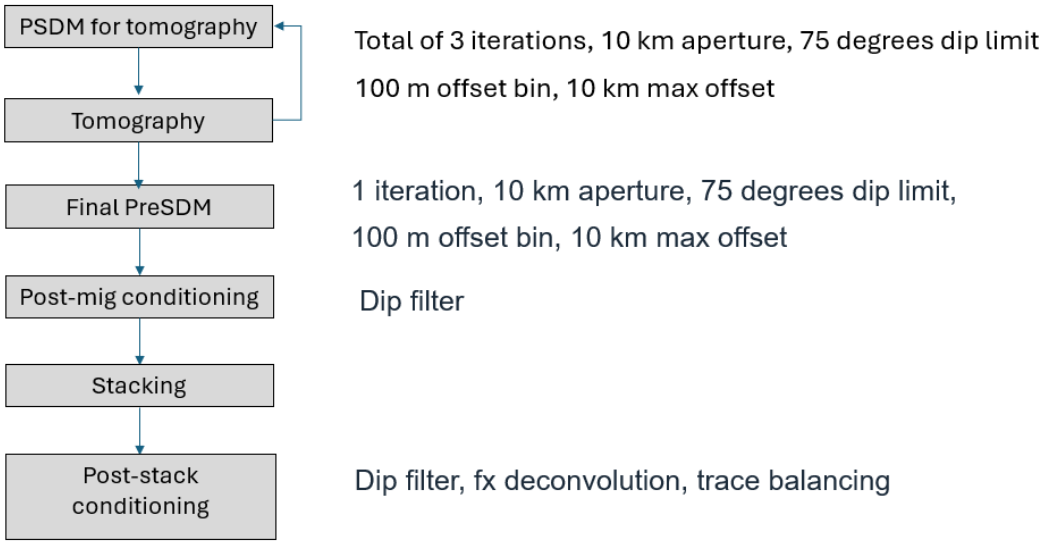

Figure 25. Depth imaging workflow.

Table 7. K-PreSDM processing flow.

K-PreSDM Processing Flow	
1.	Pre-processed data input, with AGC and removed gain $T^{1.1}$
2.	Pre-Stack Depth Migration for velocity updates, 3 iterations
3.	RMO picking and reflection tomography 3 iterations
4.	Final K-PreSDM: 5m CDP bin spacing, 10km half-aperture, 75deg dip
5.	Post-migration spatially varying top mute and AGC 10km window
6.	CDP Stack
7.	Post-stack filtering. Depth variant bandpass filter Dip filter (Tau-Pi based +-9 dip, 21 traces aperture), F-X deconvolution (9 trace aperture 2 applications), AGC 50km window (single scalar trace balance)

4.1 INITIAL VELOCITY MODEL

The velocities obtained from time imaging are transformed to interval in depth using the Dix equation. A shallow velocity model derived from refraction tomography is scaled and merged with the transformed time imaging velocity. The maximum interval velocity was clipped to 6500 m/s and the entire field was smoothed using a 1.5 km lateral and 400 m vertical smoother. This formed the initial velocity that was further refined thought several iterations of depth imaging and reflection tomography, Figure bellow.

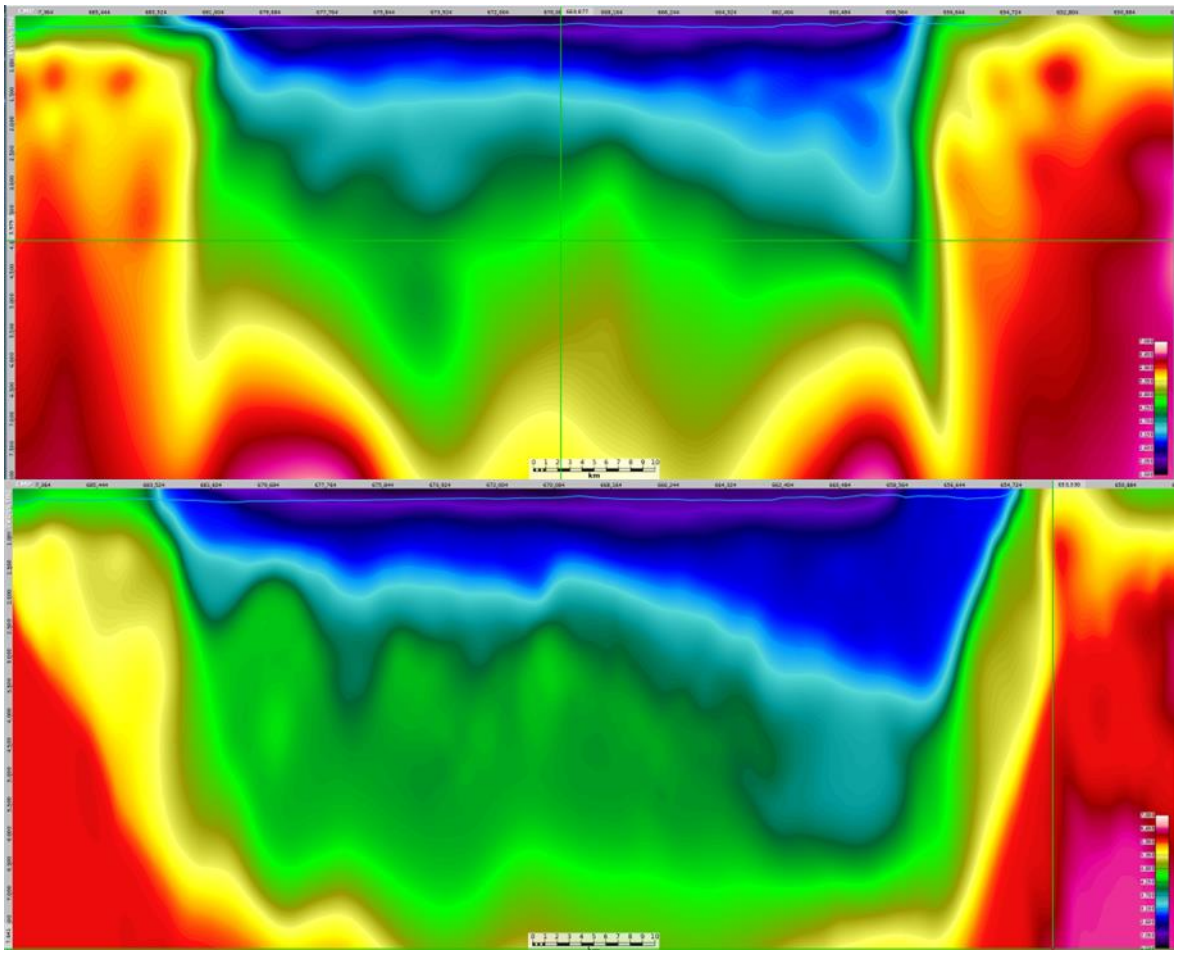

Figure 26. Starting velocity model (top), final velocity model for depth imaging (bottom).

4.2 TOMOGRAPHIC VELOCITY UPDATES

The technique of pre-stack reflection tomography involves multiple iterations of residual moveout (RMO) analysis applied to depth-migrated Common-Image-Point (CIP) gathers for updating an initial model. Automatic estimation of hyperbolic RMO is derived from CIP gathers, following the methodology detailed by Woodward et al. (2008). Initial iterations primarily focused on rectifying velocity discrepancies in shallow zones before progressing downwards to update the entire velocity model. Each subsequent iteration calculated an updated velocity model, minimizing the observed residual moveout, as described by Tanis et al. (2006). The final velocity model following 3 iterations of tomography is shown below in Figure 27 and Figure 28.

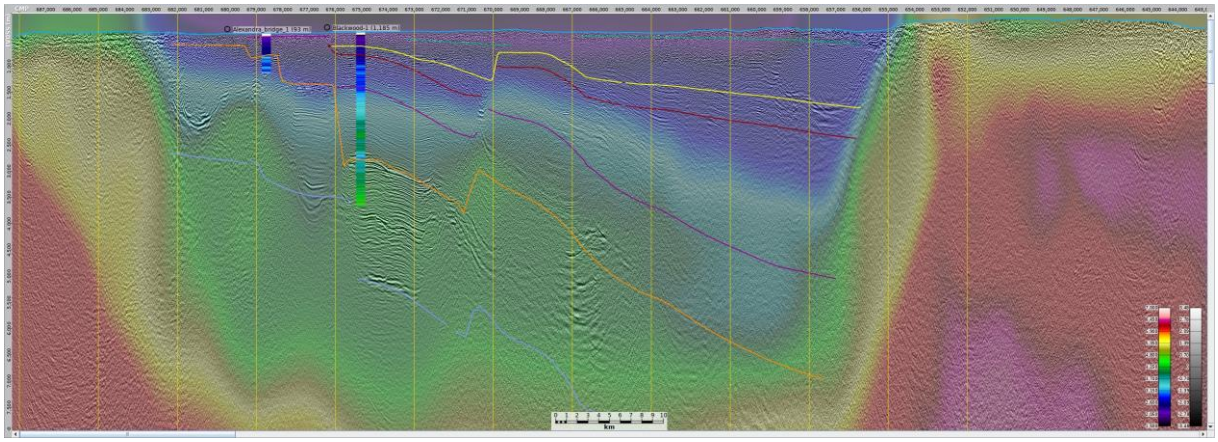

Figure 27. PSDM Stack overlain with final velocity model, GSWA-provided horizons and FWS in Perth Basin area.

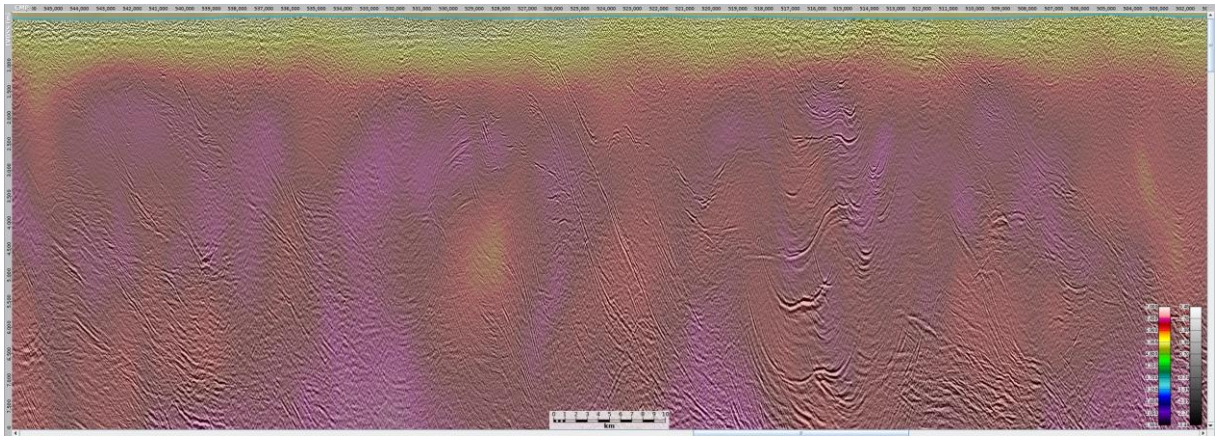

Figure 28. PSDM Stack overlain with final velocity model in a hard rock area.

To ensure accuracy, this model is compared to nearby FWS logs sourced from reliable measurements in existing drillholes (Figure 29. Close up into PSDM Stack overlain with final velocity model, provided horizons and FWS for quality control purposes.). An excellent match can be observed between the two datasets. Extrapolated, depth-converted, horizons from nearby 2D seismic lines also show good correlation with reflectivity of PreSDM stack.

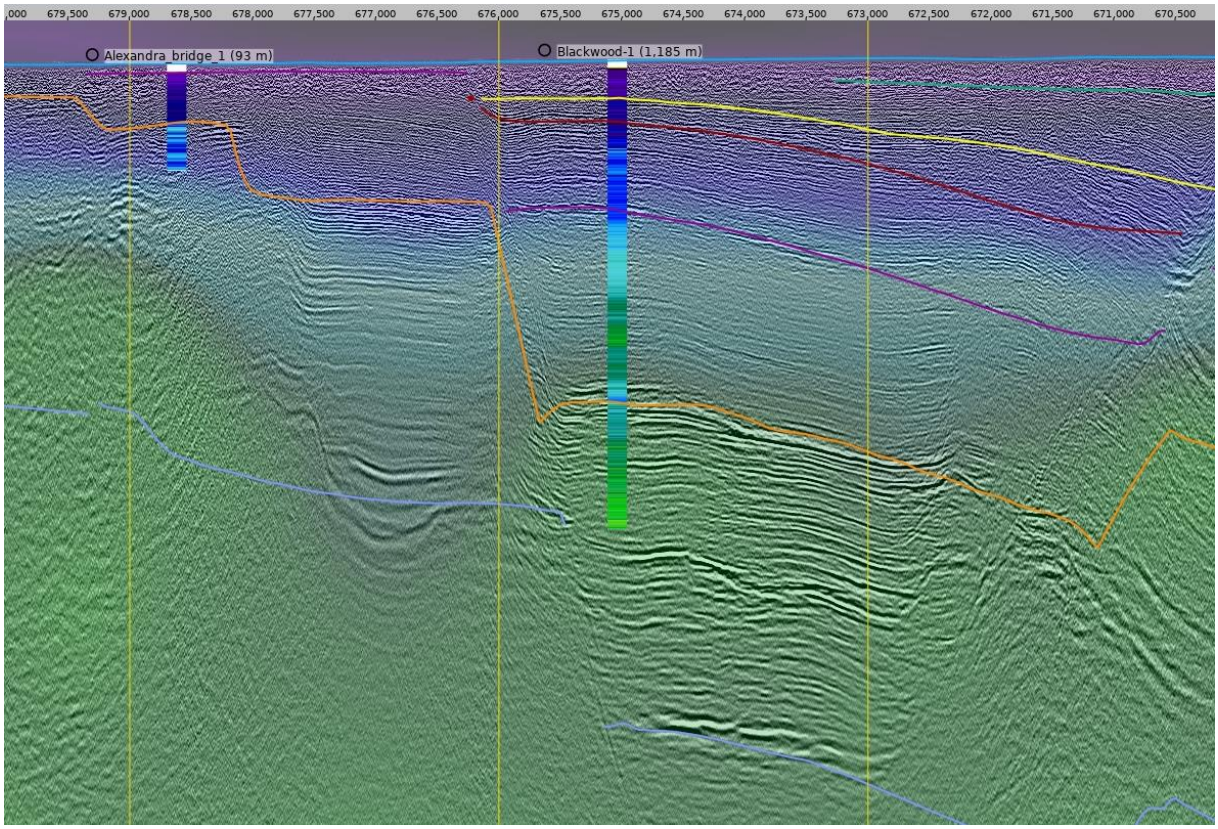

Figure 29. Close up into PSDM Stack overlain with final velocity model, provided horizons and FWS for quality control purposes.

4.3 KIRCHHOFF PRESDM

The K-PreSDM algorithm relies on ray tracing, and the seismic image is generated through diffraction summation. It demonstrates versatility by effectively handling data across a wide frequency range, particularly beneficial in scenarios where high resolution is paramount. Notably, it has fewer dip limitations and is better able to handle rapid, lateral velocity changes.

Successful implementation requires substantial S-R offsets, robust reflectivity, and Common-Image-Point (CIP) gathers that have undergone migration with a suitable initial velocity model. The accuracy of this initial velocity model, particularly in the near surface, is crucial, as a deficiency in trace fold and small S-R offsets can impede the reflection tomography's ability to update the velocity model.

Unlike with time imaging techniques, depth imaging does not require assumption of replacement velocity to migrate data from surface to final datum. As migration is in depth domain, we use measured source/receiver elevations to image data to a final flat datum of 410m. Together with accurate velocity

model and superior imaging algorithm, depth imaging provided high-precision mapping in both the hard rock and Perth Basin areas.

4.4 POST MIGRATION PROCESSING

K-PreSDM data passed through additional post-migration processes (see above in Table 7) to remove unwanted noise and artefacts on the migrated gathers and improve reflectivity of the stack. The flow included depth varying gain and bandpass filtering, random noise attenuation and coherency filtering.

4.5 FINAL PRESDM STACKS

The Figures below show full PreSDM stacks without (Figure 30) and with post-stack processing (Figure 31).

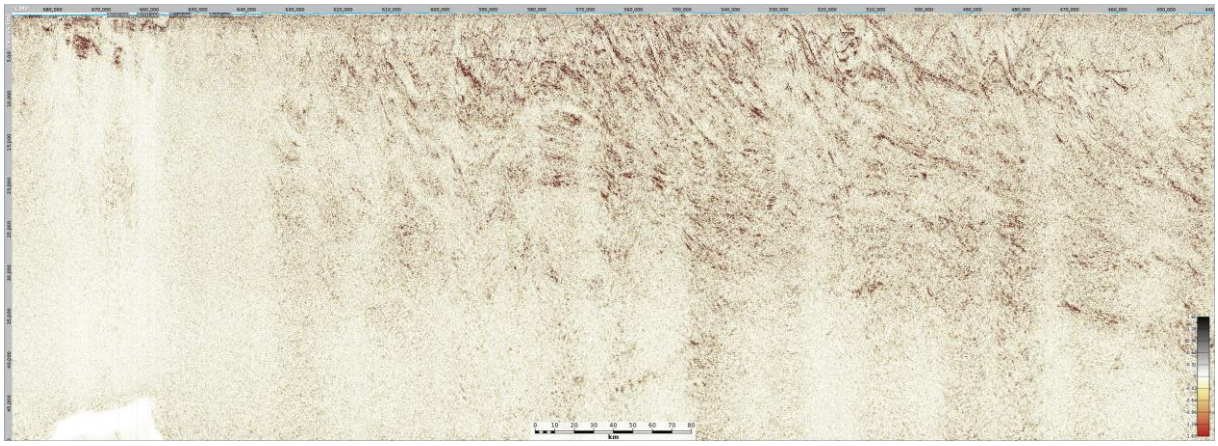

Figure 30. Raw PreSDM stack

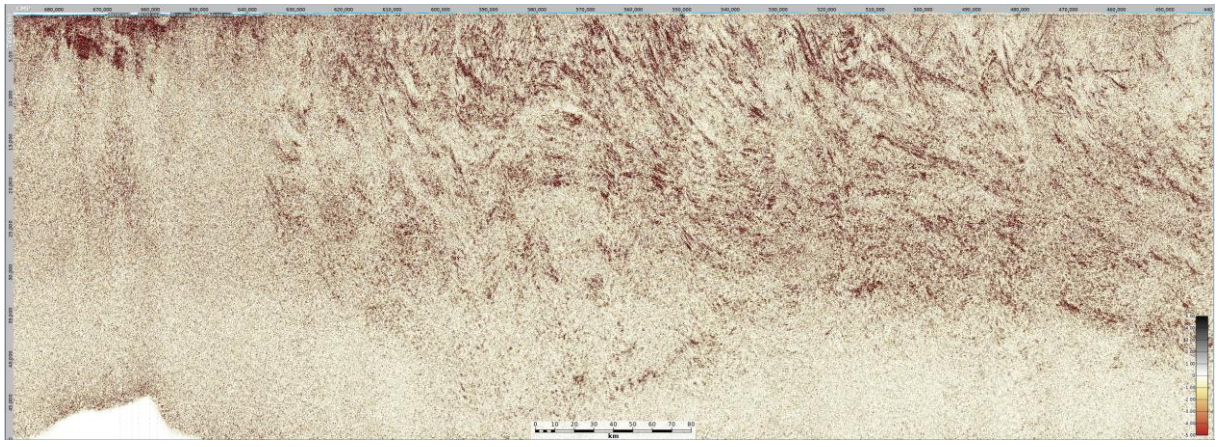

Figure 31. Final PreSDM stack

5 CONCLUSIONS

Overall, the data quality along the 23GSWA-SW1 line is considered high. While vehicle noise is spread along the length of the survey, each of the instances affected an isolated number of channels. After noise attenuation these affected channels do not appear to impact the image. The data reacquired around Nyabing was beneficial to the image in that area. The all-active acquisition which provided additional long offsets out to 27km appears to have benefited both the deep image and steeply dipping shallow events.

Seismic processing through the comprehensive pre-processing and PreSTM workflow generated two final subsurface images which focused on shallow and deep targets, respectively. The shallow image is complimented by three angle stacks, providing additional insight. The time migrated images were also supplied in depth after being converted using a smoothed version of the migration velocity.

Data was also passed through a Depth Imaging workflow which included 3 iterations of RMO picking and reflection tomography to update the velocity model. The final Kirchhoff Pre-stack Depth Migration and post-migration processing yielded significant uplift at line bends and areas of sharp lateral velocity contrast, particularly near the Darling Scarp and through the Perth Basin.

These images revealed notable features along the entire seismic line, including prominent eastward-dipping formations with significant variations observed at the boundaries of the Youanmi Terrane, South West Terrane and Perth Basin. The Moho is clearly defined to the east but becomes variably imaged as the line proceeds west. Some undulation in the depth to the Moho may be observed towards the centre of the line

Some recommendations are made for future seismic surveys.

1. Resampling for Improved Efficiency: The SW-1 seismic line represents a large dataset due to its length, high trace density, long record length, and a fine 2ms sample rate. While the 2ms sample rate was maintained throughout processing, the maximum sweep frequency used was only 96Hz. In such cases, resampling the data to 4ms can significantly improve processing runtimes and reduce disk space requirements by half. This resampling would not degrade the seismic bandwidth or resolution as the highest recoverable frequency content is well below the Nyquist frequency defined by the original 2ms sample rate. Implementing this approach in future surveys with similar acquisition parameters would enhance processing efficiency without compromising data quality.

2. Targeted Infill Shooting: The infill shots acquired on either side of exclusion zones where standard seismic acquisition was not permitted appear to have limited impact on image quality within those gaps. These additional shots could have been more strategically deployed within the Perth Basin. Several lines from different vintages within the basin exhibit consistently lower reflectivity. Future surveys in the Perth Basin might benefit from utilizing infill shots within these specific areas to potentially improve data quality and subsurface imaging.

6 PROCESSED DELIVERABLES

Table 8. Processed deliverables

Item #	File name	Description
1.	23GSWA_SW1_RawGeomFBP-Shots_FFID2-8500_20240416.sgy	Correlated shots with geometry and first break picks
2.	23GSWA_SW1_RawGeomFBP-Shots_FFID8502-17000_20240416.sgy	
3.	23GSWA_SW1_RawGeomFBP-Shots-FFID25502-34044_20240419.sgy	
4.	23GSWA_SW1_RawGeomFBP-Shots_FFID17002-25500_20240416.sgy	
5.	23GSWA_SW1_PreMigration-Gathers_part1_20240414_Time@410m.sgy	Pre-processed gathers sorted to CDP and prepared for migration
6.	23GSWA_SW1_PreMigration-Gathers_part2_20240414_Time@410m.sgy	
7.	23GSWA_SW1_PreMigration-Gathers_part3_20240414_Time@410m.sgy	
8.	23GSWA_SW1_PreMigration-Gathers_part4_20240414_Time@410m.sgy	
9.	23GSWA_SW1_PreSTM-Gathers_Raw_20240422_Time@410m.sgy	Raw gathers from PreSTM
10.	23GSWA_SW1_PreSTM-Stk_20sec_Full_Final_20240410_Depth@410m.sgy	20s record length final PreSTM stack converted to depth
11.	23GSWA_SW1_PreSTM-Stk_20sec_Full_Final_20240410_Time@410m.sgy	20s record length final PreSTM stack
12.	23GSWA_SW1_PreSTM-Stk_20sec_Full_Raw_20240410_Depth@410m.sgy	20s record length raw PreSTM stack converted to depth
13.	23GSWA_SW1_PreSTM-Stk_20sec_Full_Raw_20240410_Time@410m.sgy	20s record length raw PreSTM stack
14.	23GSWA_SW1_PreSTM-Stk_8sec_Far_Final_20240313_Depth@410m.sgy	8s record length final PreSTM far angle stack converted to depth
15.	23GSWA_SW1_PreSTM-Stk_8sec_Far_Final_20240410_Time@410m.sgy	8s record length final PreSTM far angle stack
16.	23GSWA_SW1_PreSTM-Stk_8sec_Far_Raw_20240313_Depth@410m.sgy	8s record length raw PreSTM far angle stack converted to depth
17.	23GSWA_SW1_PreSTM-Stk_8sec_Far_Raw_20240410_Time@410m.sgy	20s record length raw PreSTM far angle stack
18.	23GSWA_SW1_PreSTM-Stk_8sec_Full_Final_20240313_Depth@410m.sgy	
19.	23GSWA_SW1_PreSTM-Stk_8sec_Full_Final_20240422_Time@410m.sgy	
20.	23GSWA_SW1_PreSTM-Stk_8sec_Full_Raw_20240313_Depth@410m.sgy	
21.	23GSWA_SW1_PreSTM-Stk_8sec_Full_Raw_20240422_Time@410m.sgy	

22. 23GSWA_SW1_PreSTM-Stk_8sec_Mid_Final_20240410_Time@410m.sgy	
23. 23GSWA_SW1_PreSTM-Stk_8sec_Mid_Final_20240420_Depth@410m.sgy	
24. 23GSWA_SW1_PreSTM-Stk_8sec_Mid_Raw_20240410_Time@410m.sgy	
25. 23GSWA_SW1_PreSTM-Stk_8sec_Mid_Raw_20240420_Depth@410m.sgy	
26. 23GSWA_SW1_PreSTM-Stk_8sec_Near_Final_20240313_Depth@410m.sgy	
27. 23GSWA_SW1_PreSTM-Stk_8sec_Near_Final_20240410_Time@410m.sgy	
28. 23GSWA_SW1_PreSTM-Stk_8sec_Near_Raw_20240313_Depth@410m.sgy	
29. 23GSWA_SW1_PreSTM-Stk_8sec_Near_Raw_20240410_Time@410m.sgy	
30. 23GSWA_SW1_Final_PreSTM_Vel_RMST_20240312@410m.sgy	
31. 23GSWA_SW1_PreSTM_Time-Depth_Vel_RMST_20240312@410m.sgy	
32. 23GSWA_SW1_Final_PreSTM_Vel_VINTZ_20240312@410m.sgy	
33. 23GSWA_SW1_PreSDM-Gathers_Raw_part1_22042024@410m.sgy	
34. 23GSWA_SW1_PreSDM-Gathers_Raw_part2_22042024@410m.sgy	
35. 23GSWA_SW1_PreSDM-Stk_Final_v3_22042024@410m.sgy	
36. 23GSWA_SW1_Final_PreSDM_Vel_VINTZ_20240312@410m.sgy	
37. GSWA_SW1_TOP_ROCK_Rays_20231130_depth@410.sgy	
38. GSWA_SW1_TOP_ROCK_Vel_VINTZ_20231130_depth@410.sgy	

7 REFERENCES

Robinson, E.A., Treitel, S., 2008, Digital Imaging and Deconvolution: The ABCs of Seismic Exploration and Processing.

Tanis, M. C., H. Shah, P. A. Watson, M. Harrison, S. Yang, L. Lu, and C. Carvill, 2006, Diving-wave refraction tomography and reflection tomography for velocity model building: 76th Annual International Meeting, SEG, Expanded Abstracts, 3340–3344, http://dx.doi.org/10.1190/1.2370225.

Woodward M. J., D. Nichols, O. Zdraveva, P. Whitfield, and T. Johns, 2008, A decade of tomography: Geophysics, 73, no. 5, VE5–VE11.

Yilmaz, O, 2001, Seismic data analysis: Society of Exploration Geophysicists.

Ziramov, S., Young, C., Kinkela, J., Turner, G. & Urosevic, M. (2023) Pre-stack depth imaging techniques for the delineation of the Carosue Dam gold deposit, Western Australia. Geophysical Prospecting, 00, 1– 19. https://doi.org/10.1111/1365-2478.13314

8 APPENDIX

8.1 SEGY HEADERS - FIELD SHOTS

See accompanying INOVA trace header specifications document.

INOVA Disk Tape and Tape Image Formats 7D.pdf

8.2 SEGY HEADERS - GEOM FBP SHOTS, PRE-MIG GATHERS

Table 9. SEGY headers for Geom, FBP shots and pre-migration gathers

Header	Byte location	Description
SOU_STN	17-20	Source station
CDP	21-24	CDP number
CDP_FOLD	33-34	Fold of CDP
OFFSET	37-40	Distance from source to receiver
REC_ELEV	41-44	Surface elevation at receiver
SOU_ELEV	45-48	Surface elevation at source
REC_DATUM	53-56	Final datum elevation at receiver (410 m)
SOU_DATUM	57-60	Final datum elevation at source (410 m)
SOU_X	73-76	Source X coordinate
SOU_Y	77-80	Source Y coordinate
REC_X	81-84	Receiver X coordinate
REC_Y	85-88	Receiver Y coordinate
WVEL	91-92	Weathering velocity (1000 m/s)
SUBWVEL	93-94	Sub-weathering velocity
SOU_STAT	99-100	Source refraction static to final datum
REC_STAT	101-102	Receiver refraction static to final datum
TOT_STAT	103-104	Total static applied
CDP_X	181-184	CDP X coordinate
CDP_Y	185-188	CDP Y coordinate
CDP_STN	191-194	CDP station
REC_STN	195-198	Receiver station
CDP_ELEV	211-212	Surface elevation of CDP
REF_DEPTH	215-216	Refractor depth at receiver
REF_ELEV	217-218	Refractor elevation at receiver
REP_VEL	219-220	Replacement velocity (5800 m/s)
FNL_STAT	225-226	Static to move from floating to final datum
FB_PICK	237-240	First break pick time

8.3 SEGY HEADERS - MIGRATED GATHERS AND STACKS

Table 10. SEGY headers for migrated gathers and stacks

Header	Byte location	Description
SOU_STN	17-20	Source station
CDP	21-24	CDP number
CDP_FOLD	33-34	Fold of CDP
OFFSET	37-40	Migrated offset bin centre
REC_DATUM	53-56	Final datum elevation at receiver (410 m)
SOU_DATUM	57-60	Final datum elevation at source (410 m)
CDP_X	73-76	CDP X coordinate
CDP_Y	77-80	CDP Y coordinate
WVEL	91-92	Weathering velocity (1000 m/s)
SUBWVEL	93-94	Sub-weathering velocity
CDP_X	181-184	CDP X coordinate
CDP_Y	185-188	CDP Y coordinate
CDP_STN	191-194	CDP station
REC_STN	195-198	Receiver station
CDP_ELEV	211-212	Surface elevation of CDP
REF_ELEV	217-218	Refractor elevation at receiver
REP_VEL	219-220	Replacement velocity (5800 m/s)
TOT_STAT	223-224	Total static applied
FNL_STAT	225-226	Static to move from floating to final datum

8.4 ACCOMPANYING TEST REPORTS AND WEEKLY UPDATES

Table 11. Test reports and weekly updates

Item #	File name
1.	20231102_GSWA_SW1_Processing_kickoff.pdf
2.	20231121_GSWA_SW1_ProcessingUpdate.pdf
3.	20231128_GSWA_SW1_ProcessingUpdate.pdf
4.	20231205_GSWA_SW1_ProcessingUpdate.pdf
5.	20231205_GSWA_SW1_TopRock_RefractionTomography.pdf
6.	20231212_GSWA_SW1_ProcessingUpdate.pdf
7.	20231219_GSWA_SW1_ProcessingUpdate.pdf
8.	20240109_GSWA_SW1_ProcessingUpdate.pdf
9.	20240116_GSWA_SW1_ProcessingUpdate.pdf
10.	20240123_GSWA_SW1_ProcessingUpdate.pdf
11.	20240130_GSWA_SW1_ProcessingUpdate.pdf
12.	20240130_GSWA_SW1_PSDM_imaging_update_20240326.pdf
13.	20240130_GSWA_SW1_PSDM_imaging_update_20240402.pdf
14.	20240206_GSWA_SW1_ProcessingUpdate.pdf
15.	20240206_GSWA_SW1_PSDM_feasibility_study.pdf
16.	20240213_GSWA_SW1_ProcessingUpdate_v2.pdf
17.	20240227_GSWA_SW1_ProcessingUpdate.pdf
18.	20240305_GSWA_SW1_ProcessingUpdate.pdf
19.	20240409_GSWA_SW1_PSDM_imaging_update.pdf
20.	20240416_GSWA_SW1_Geological_QC_V2.pdf
21.	20240416_GSWA_SW1_ProcessingUpdate.pdf
22.	20240416_GSWA_SW1_PSDM_imaging_update.pdf
23.	20240430_GSWA_SW1_PreSDM_update.pdf

8.5 SEISOMICS

Title: Revealing Geological Details in Hard Rock Seismic Volumes using Medical Imaging Technology

Abstract: We present "Seisomics", a machine-learning workflow to segment and classify seismic imaging data into domains of similar statistical texture. This approach has been adapted from medical imaging; customizing the image feature sets from the Image Biomarker Standardisation Initiative (IBSI) V1 for application on 3D and 2D seismic datasets. The method aims to "discriminate potentially meaningful differences in imaging which are not readily apparent to the human eye". This is first performed by computing a textural and co-located petrophysical attributes and then applying classification algorithms. This segments the imaging volume into regions. Where dimensionality reduction algorithms can be applied to improve classification with higher dimensionality datasets. This method aims to reveal high-resolution geological details in the near-surface, imaging subtle transitions in geochemistry or geology.

Co-Authors:
1. Dr. Andrew M. Pethick*, HiSeis, A.Pethick@hiseis.com

2. Mrs. Sian Bright, HiSeis, S.Bright@hiseis.com

3. Mr. Jeremy Smith, HiSeis, J.Smith@hiseis.com

Address For all Authors: HiSeis Pty Ltd, 140 Hay Street, Subiaco, Western Australia

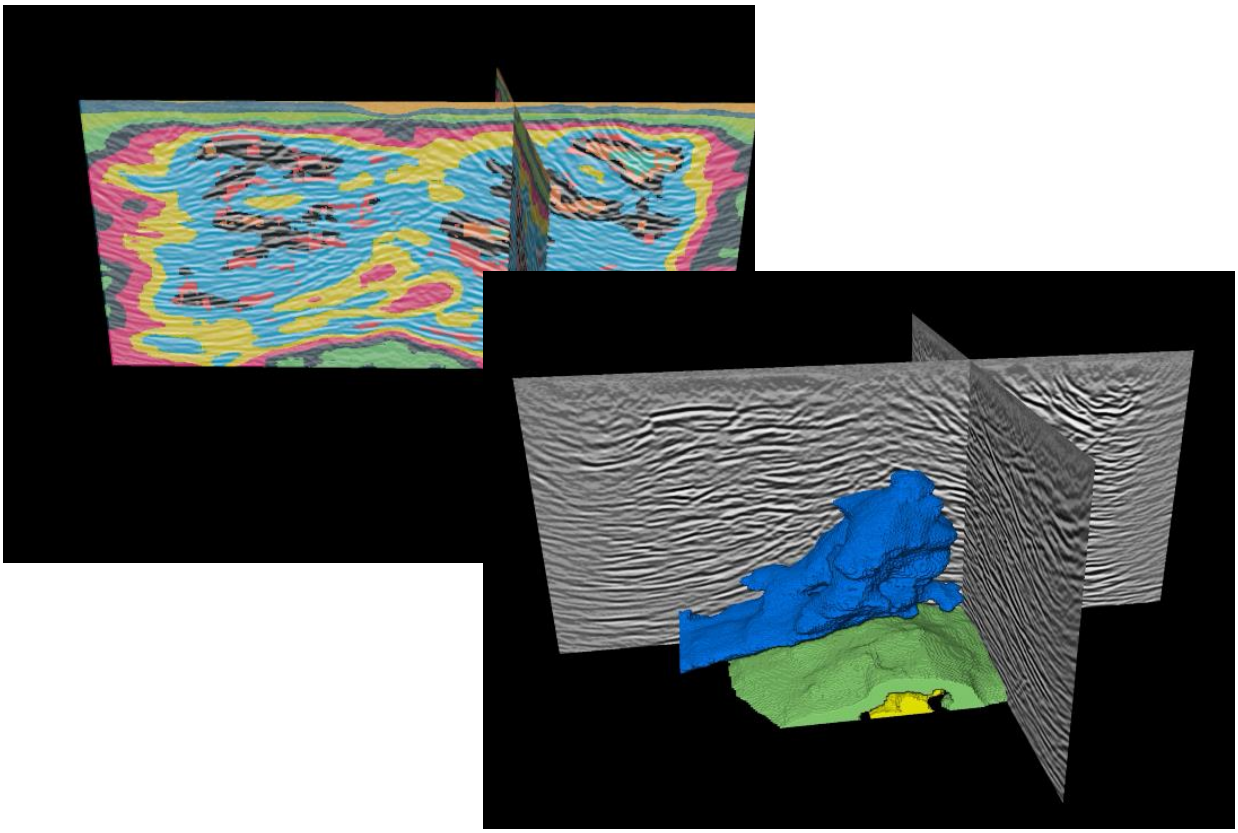

HiSeis

hiseis.com

140 Hay Street, Subiaco WA 6008

+61 8 9470 9866